Mössbauer, EPR, and ENDOR Studies of the Hydroxylase and Reductase Components of Methane Monooxygenase from *Methylosinus trichosporium* OB3b

Brian G. Fox,[†] Michael P. Hendrich,[‡] Kristene K. Surerus,[†] Kristoffer K. Andersson,[‡] Wayne A. Froland,[‡] John D. Lipscomb,*[,‡] and Eckard Münck*[,†]

Contribution from the Department of Chemistry, Carnegie Mellon University, Pittsburgh, Pennsylvania 15213, and Department of Biochemistry, University of Minnesota, Minneapolis, Minnesota 55455

Received October 19, 1992

Abstract: Soluble methane monooxygenase (MMO) isolated from *Methylosinus trichosporium* OB3b consists of three components: hydroxylase, reductase, and component B. The active-site diiron cluster of the hydroxylase has been studied with Mössbauer, ENDOR, and EPR spectroscopies. Mössbauer spectra of the oxidized cluster show that the two high-spin irons are antiferromagnetically coupled in accord with our preliminary study (Fox et al. *J. Biol. Chem.* **1988**, *263*, 10553-10556). Mössbauer studies also reveal the presence of two cluster conformations at pH 9. The excited-state $S = 2$ multiplet of the exchange-coupled cluster (Fe^{3+}·Fe^{3+}) gives rise to an integer-spin EPR signal near $g = 8$; this is the first quantitative study of such a signal from any system. Analysis of the temperature dependence of the $g = 8$ signal yields $J = 15 \pm 5$ cm^{-1} for the exchange-coupling constant ($H_{ex} = J\mathbf{S}_1\cdot\mathbf{S}_2$). This value is more than 1 order of magnitude smaller than those reported for the oxo-bridged clusters of hemerythrin and *Escherichia coli* ribonucleotide reductase ($H_{ex} = J\mathbf{S}_1\cdot\mathbf{S}_2$, $J = 270$ and 220 cm^{-1}, respectively), suggesting that the bridging ligand of the hydroxylase cluster is not an unsubstituted oxygen atom. Mössbauer spectra of the hydroxylase in applied fields of up to 8 T reveal a paramagnetic admixture of a low-lying excited state into the ground singlet. Both the spectral shape and intensity are well represented by assuming that the spin expectation values for the cluster sites increase linearly with magnetic field. However, the origin of this effect is not fully explicable in the framework of the standard spin Hamiltonian including zero-field splittings and antisymmetric exchange. EPR studies of the uncomplexed mixed valence (Fe^{3+}·Fe^{2+}) hydroxylase show that it is composed of two slightly different cluster forms in an approximate 4:1 ratio. The zero-field splitting (ZFS) of the ferrous site of the mixed valence hydroxylase is sensitive to complexation with products or inhibitors, while complexation by the component B perturbs the exchange coupling. The binding of the inhibitor dimethyl sulfoxide results in the smallest distribution of ZFS parameters and thus is investigated here in a correlated study using each of the three spectroscopic techniques. The data were analyzed with a spin Hamiltonian that includes exchange coupling ($J = 60$ cm^{-1}) and mixing of multiplets by zero-field splittings. The analysis shows that the orbital ground state of the ferrous site has predominantly d_{xy} symmetry; the z-axis of this orbital points along the z-direction of the cluster **g**-tensor. Mössbauer and ^{57}Fe-ENDOR spectra indicate that the **A**-tensor of the ferric site is anisotropic; the ^{57}Fe-ENDOR signals are the first reported for diiron–oxo clusters. Analysis of the Mössbauer spectra of the uncomplexed, reduced (Fe^{2+}·Fe^{2+}) hydroxylase cluster recorded in strong applied fields (up to 6.0 T) unambiguously shows that the two iron sites are inequivalent. Spectra of the oxidized cluster are also best fit by assuming that the irons of the cluster reside in inequivalent environments. Considered in light of the overall two-fold symmetry of hydroxylase revealed by ongoing structural studies, the present findings show that the hydroxylase contains two, probably identical, active-site diiron clusters whose individual iron atoms are structurally distinct. Mössbauer and EPR spectra of the $[2Fe\text{–}2S]^{2+,1+}$ cluster of the MMO reductase component are also reported and analyzed.

Soluble methane monooxygenase (MMO, EC 1.14.13.25) consists of three protein components: a 40-kDa reductase containing both FAD and a [2Fe2S] cluster; a 16-kDa protein termed component B containing no metals or organic cofactors; and a 245-kDa hydroxylase (quaternary structure $(\alpha\beta\gamma)_2$) containing up to 4 mol of iron.[1] Soluble MMO catalyzes the O_2-dependent oxidation of methane to methanol.[2] In addition, a wide variety of other hydrocarbons are adventitiously oxidized.[3] Efficient reconstitution of NADH-linked catalytic turnover requires all three protein components.[4] However, in the absence of the other components, the hydroxylase is able to catalyze hydroxylation reactions either upon chemical reduction and exposure[1a,4b] to O_2 or upon addition[4b,5] of H_2O_2, demonstrating that the complete active site required for oxygenase catalysis resides on the hydroxylase alone.

All EPR and Mössbauer studies conducted to date are consistent with the presence of a spin-coupled diiron cluster in the hydroxylase active site.[1] Iron quantitation in combination with the observation

* Authors to whom correspondence should be directed.
[†] Carnegie Mellon University.
[‡] University of Minnesota.

(1) (a) Fox, B. G.; Froland, W. A.; Dege, J. E.; Lipscomb, J. D. *J. Biol. Chem.* **1989**, *264*, 10023-10033. (b) Froland, W. F.; Andersson, K. K.; Lee, S.-K.; Liu, Y.; Lipscomb, J. D. In *Applications of Enzyme Biotechnology*; Kelly, J. W., Baldwin, T. O., Eds.; Plenum Press: New York, 1991; pp 39-53. (c) Fox, B. G.; Lipscomb, J. D. In *Biological Oxidation Systems*; Reddy, C. C., Hamilton, G. A., Madyastha, K. M., Eds.; Academic Press: New York, 1990; Vol. 1, pp 367-388.

(2) Dalton, H. *Adv. Appl. Microbiol.* **1980**, *26*, 71-87.

(3) (a) Rataj, M. J.; Knauth, J. E.; Donnelly, M. I. *J. Biol. Chem.* **1991**, *266*, 18684-18690. (b) Fox, B. G.; Borneman, J. G.; Wackett, L. P.; Lipscomb, J. D. *Biochemistry* **1990**, *29*, 6419-6427. (c) Ruzicka, F.; Huang, D.-S.; Donnelly, M. I.; Frey, P. A. *Biochemistry* **1990**, *29*, 1696-1700. (d) Green, J.; Dalton, H. *J. Biol. Chem.* **1989**, *246*, 17698-17703.

(4) (a) Fox, B. G.; Liu, Y.; Dege, J. E.; Lipscomb, J. D. *J. Biol. Chem.* **1991**, *266*, 540-550. (b) Froland, W. A.; Andersson, K. K.; Lee, S.-K.; Liu, Y.; Lipscomb, J. D. *J. Biol. Chem.* **1992**, *267*, 17588-17597. (c) Green, J.; Dalton, H. *J. Biol. Chem.* **1985**, *260*, 15795-15801.

(5) Andersson, K. K.; Froland, W. A.; Lee, S.-K.; Lipscomb, J. D. *New J. Chem.* **1991**, *15*, 411-415.

0002-7863/93/1515-3688$04.00/0

of a single spectroscopically distinct type of iron environment for the *Methylosinus trichosporium* OB3b enzyme indicated that two diiron clusters are present.[1a] In contrast, the analogous hydroxylase prepared from *Methylococcus capsulatus* (Bath) reportedly contains only a single cluster.[6] Similar, but not identical clusters[7] are found in a functionally diverse group of proteins including hemerythrin,[8] ribonucleotide reductase,[9] rubrerythrin,[10] and the purple acid phosphatases including uteroferrin.[11] In addition, a number of synthetic model complexes[12] that mimic the structural[13] or catalytic properties[14] of these proteins have been produced and characterized as well.

Since both oxygen activation and substrate hydroxylation activities of MMO apparently occur at the hydroxylase diiron cluster, a description of the detailed mechanism of biological methane oxidation will require corresponding structural characterization of this diiron cluster. Of the proteins currently known to contain diiron clusters, only the hydroxylase is capable of catalytic oxygenase activity,[15] implying a unique contribution of this specific cluster structure to the catalytic process.

A wide variety of methods including optical,[1a] EPR,[1a,4a,16] Mössbauer,[16a] EXAFS,[6a,16c] ENDOR,[17] MCD,[18] and resonance Raman[19] spectroscopies has been utilized to characterize the hydroxylase. In the present study, characteristic structural properties of the hydroxylase diiron cluster are revealed through the use of Mössbauer spectroscopy in combination with ^{57}Fe-ENDOR and integer- and half-integer-spin EPR spectroscopies. For each of the three redox states in which the hydroxylase cluster can be observed, the two iron atoms are spin-coupled and present in distinguishable environments. When considered in the light of on-going protein structural studies, the present results definitively show that the hydroxylase contains two, probably identical, active-site diiron clusters. Analysis of the hydroxylase spectra with a spin Hamiltonian formalism provides a convenient basis for comparison with the similarly analyzed spectra of other proteins containing diiron clusters. In accord with our preliminary studies,[16a] the spectra of the hydroxylase are readily distinguishable from those of the other proteins containing diiron clusters. Perhaps most importantly, the magnitude of the spin coupling in the diferric state is significantly smaller than the values observed for other well-studied proteins such as hemerythrin and ribonucleotide reductase. The possible implications of this weak coupling for the unusual spectral properties of hydroxylase, the nature of the bridging ligand, and the participation of the diiron cluster in catalysis are discussed. The hydroxylase is also shown to differ from other diiron proteins in that factors such as ligand[17,19] or remote component B binding[4a] as well as pH or temperature appear to significantly perturb the cluster environment. These effects may be related to protein conformational changes occurring during the hydroxylase catalytic cycle that have been revealed by related studies of turnover kinetics[4a] and conformationally sensitive alterations in product distribution.[4b]

Materials and Methods

Protein Purification and Characterization. The growth of *M. trichosporium* OB3b and the purification and physical characterization of the MMO components were as previously described.[1a,20] The hydroxylase used for Mössbauer and ^{57}Fe-ENDOR studies was purified from bacteria grown in media containing ^{57}Fe (95.5% isotopic purity, ICON, Summit, NJ) as the sole source of iron. The protein preparations exhibited the following physical properties: hydroxylase, 1000–1700 mU/mg of protein, 3.8 ± 0.3 Fe/mol; component B, 10 000 mU/mg; reductase, 25 000 mU/mg, 2.1 ± 0.1 Fe/mol, 1 FAD/mol. Catalytic activities were determined as previously described.[20]

Preparation of Hydroxylase Samples. Mössbauer samples of the oxidized hydroxylase consisted of nominally 300 μL of 1 mM protein. Samples containing methanol (50 mM) or Me_2SO (300 mM) were equilibrated at 25 °C for 10 min before freezing in liquid nitrogen. For pH adjustment, the oxidized hydroxylase in 25 mM MOPS, pH 7, with 5% (v/v) glycerol was diluted with 2 M MOPS, pH 7, or 2 M TAPS, pH 9, to make a final buffer concentration of 150 mM at the respective pH value. Parallel Mössbauer and EPR samples of the mixed-valence and reduced hydroxylase were prepared under anaerobic conditions as

(6) (a) DeWitt, J. G.; Bentsen, J. G.; Rosenzweig, A. C.; Hedman, B.; Green, J.; Pilkington, S.; Papaefthymiou, G. C.; Dalton, H.; Hodgson, K. O.; Lippard, S. J. *J. Am. Chem. Soc.* **1991**, *113*, 9219–9235. (b) Woodland, M. P.; Dalton, H. *J. Biol. Chem.* **1984**, *259*, 53–59.

(7) (a) Que, L., Jr.; True, A. E. In *Progress in Inorganic Chemistry: Bioinorganic Chemistry*; Lippard, S. J., Ed.; John Wiley & Sons: New York, 1990; Vol. 38, pp 97–200. (b) Vincent, J. B.; Olivier-Lilley, G. C.; Averill, B. A. *Chem. Rev.* **1990**, *90*, 1447–1467. (c) Sanders-Loehr, J. In *Iron Carriers and Iron Proteins*; Loehr, T. M., Ed.; VCH: New York, 1989; pp 375–466. (d) Que, L., Jr.; Scarrow, R. C. In *Metal Clusters in Proteins*; Que, L., Jr., Ed.; ACS Symposium Series No. 372; American Chemical Society: Washington, DC, 1988; pp 152–178.

(8) (a) Hendrich, M. P.; Pearce, L. L.; Que, L., Jr.; Chasteen, N. D.; Day, E. P. *J. Am. Chem. Soc.* **1991**, *113*, 3039–3044. (b) McCormick, J. M.; Reem, R. C.; Solomon, E. I. *J. Am. Chem. Soc.* **1991**, *113*, 9066–9079. (c) Reem, R. C.; McCormick, J. M.; Richardson, D. E.; Devlin, F. J.; Stephens, P. J.; Musselman, R. L.; Solomon, E. I. *J. Am. Chem. Soc.* **1989**, *111*, 4688–4704. (d) Nocek, J. M.; Kurtz, D. M., Jr.; Sage, J. T.; Xia, Y.-M.; Debrunner, P. G.; Schiemke, A. K.; Sanders-Loehr, J.; Loehr, T. M. *Biochemistry* **1988**, *27*, 1014–1024. (e) Reem, R. C.; Solomon, E. I. *J. Am. Chem. Soc.* **1987**, *109*, 1216–1226. (f) Pearce, L. L.; Kurtz, D. M., Jr.; Xia, Y.-M.; Debrunner, P. G. *J. Am. Chem. Soc.* **1987**, *109*, 7286–7293. (g) Stenkamp, R. E.; Sieker, L. C.; Jensen, L. H. *J. Am. Chem. Soc.* **1984**, *106*, 618–622. (h) Dawson, J. W.; Gray, H. B.; Hoenig, H. E.; Rossman, G. R.; Shredder, J. M.; Wang, R.-H. *Biochemistry* **1972**, *11*, 461–465. (i) Garbett, K.; Johnson, C. E.; Klotz, I. M.; Okamura, M. Y.; Williams, R. J. P. *Arch. Biochem. Biophys.* **1971**, *142*, 574–583.

(9) (a) Lynch, J. B.; Juarez-Garcia, C.; Münck, E.; Que, L., Jr. *J. Biol. Chem.* **1989**, *264*, 8091–8096. (b) Nordlund, P.; Sjöberg, B.-M.; Eklund, H. *Nature* **1990**, *345*, 593–598. (c) Elgren, T. E.; Lynch, J. B.; Juarez-Garcia, C.; Münck, E.; Sjöberg, B.-M.; Que, L., Jr. *J. Biol. Chem.* **1991**, *266*, 19265–19268. (d) Bollinger, J. M., Jr.; Stubbe, J.; Huynh, B. H.; Edmondson, D. E. *J. Am. Chem. Soc.* **1991**, *113*, 6289–6291. (e) Bollinger, J. M., Jr.; Edmondson, D. E.; Huynh, B.-H.; Filley, J.; Norton, J. R.; Stubbe, J. *Science* **1991**, *253*, 292–298. (f) Sahlin, M.; Sjöberg, B.-M.; Backes, G.; Loehr, T.; Sanders-Loehr, J. *Biochem. Biophys. Res. Commun.* **1990**, *167*, 813–818. (g) Petersson, L.; Gräslund, A.; Ehrenberg, A.; Sjöberg, B.-M.; Reichard, P. *J. Biol. Chem.* **1980**, *255*, 6706–6712. (h) Atkin, C. I.; Thelander, L.; Reichard, P.; Lang, G. *J. Biol. Chem.* **1973**, *248*, 7464–7472.

(10) LeGall, J.; Prickril, B. C.; Moura, I.; Xavier, A. V.; Moura, J. J. G.; Huynh, B.-H. *Biochemistry* **1988**, *27*, 1636–1642.

(11) (a) Sage, J. T.; Xia, Y.-M.; Debrunner, P. G.; Keough, D. T.; de Jersey, J.; Zerner, B. *J. Am. Chem. Soc.* **1989**, *111*, 7239–7247. (b) Day, E. P.; David, S. S.; Peterson, J.; Dunham, W. R.; Bonvoisin, J. J.; Sands, R. H.; Que, L., Jr. *J. Biol. Chem.* **1988**, *263*, 15561–15567. (c) Averill, B. A.; Davis, J. C.; Burman, S.; Zirino, T.; Sanders-Loehr, J.; Loehr, T. M.; Sage, J. T.; Debrunner, P. G. *J. Am. Chem. Soc.* **1987**, *109*, 3760–3767.

(12) (a) Lippard, S. J. *Angew. Chem., Int. Ed. Engl.* **1988**, *27*, 344–361. (b) Kurtz, D. M., Jr. *Chem. Rev.* **1990**, *90*, 585–606.

(13) (a) Ménage, S.; Zang, Y.; Hendrich, M. P.; Que, L., Jr. *J. Am. Chem. Soc.* **1992**, *114*, 7786–7792. (b) Tolman, W. B.; Liu, S.; Bentsen, J. G.; Lippard, S. J. *J. Am. Chem. Soc.* **1991**, *113*, 152–164. (c) Borovik, A. S.; Papaefthymiou, V.; Taylor, L. F.; Anderson, O. P.; Que, L., Jr. *J. Am. Chem. Soc.* **1989**, *111*, 6183–6195. (d) Borovik, A. S.; Que, L., Jr. *J. Am. Chem. Soc.* **1988**, *110*, 2345–2347. (e) Hartman, J. R.; Rardin, R. L.; Chaudhuri, P.; Pohl, K.; Wieghardt, K.; Nuber, B.; Weiss, J.; Papaefthymiou, G. C.; Frankel, R. B.; Lippard, S. J. *J. Am. Chem. Soc.* **1987**, *109*, 7387–7396. (f) Armstrong, W. H.; Spool, A.; Papaefthymiou, G. C.; Frankel, R. B.; Lippard, S. J. *J. Am. Chem. Soc.* **1984**, *106*, 3653–3667.

(14) (a) Leising, R. L.; Brennan, B. A.; Que, L., Jr.; Fox, B. G.; Münck, E. *J. Am. Chem. Soc.* **1991**, *113*, 3988–3990. (b) Stassinopoulos, A.; Schulte, G.; Papaefthymiou, G. C.; Caradonna, J. P. *J. Am. Chem. Soc.* **1991**, *113*, 8686–8697. (c) Leising, R. A.; Norman, R. E.; Que, L., Jr. *Inorg. Chem.* **1990**, *29*, 2553–2555. (d) Stassinopoulos, A.; Caradonna, J. P. *J. Am. Chem. Soc.* **1990**, *112*, 7071–7073. (e) Vincent, J. B.; Huffman, J. C.; Christou, G.; Li, Q.; Nanny, M. A.; Hendrickson, D. N.; Fong, R.; Fish, R. *J. Am. Chem. Soc.* **1988**, *110*, 6898–6900. (f) Murch, B. P.; Bradley, F. C.; Que, L., Jr. *J. Am. Chem. Soc.* **1986**, *108*, 5027–5028.

(15) Site-specific mutation of ribonucleotide reductase Phe-208 to Tyr has converted this protein to a self-hydroxylating monooxygenase, resulting in enzyme inactivation. Ormö, M.; deMaré, F.; Regnström, K.; Aberg, A.; Sahlin, M.; Ling, J.; Loehr, T. M.; Sanders-Loehr, J.; Sjöberg, B.-M. *J. Biol. Chem.* **1992**, *267*, 8711–8714.

(16) (a) Fox, B. G.; Surerus, K. K.; Münck, E.; Lipscomb, J. D. *J. Biol. Chem.* **1988**, *263*, 10553–10556. (b) Hendrich, M. P.; Münck, E.; Fox, B. G.; Lipscomb, J. D. *J. Am. Chem. Soc.* **1990**, *112*, 5861–5865. (c) Prince, R. C.; George, G. N.; Savas, J. C.; Cramer, S. P.; Patel, R. N. *Biochem. Biophys. Acta* **1988**, *952*, 220–229. (d) Woodland, M. P.; Patil, D. S.; Cammack, R.; Dalton, H. *Biochem. Biophys. Acta* **1986**, *873*, 237–242.

(17) Hendrich, M. P.; Fox, B. G.; Andersson, K. K.; Debrunner, P. G.; Lipscomb, J. D. *J. Biol. Chem.* **1992**, *267*, 261–269.

(18) Solomon, E. I.; Zhang, Y. *Acc. Chem. Res.* **1992**, *25*, 343–352.

(19) Andersson, K. K.; Elgren, T. E.; Que, L., Jr.; Lipscomb, J. D. *J. Am. Chem. Soc.* **1992**, *114*, 8711–8713.

(20) Fox, B. G.; Froland, W. A.; Jollie, D. R.; Lipscomb, J. D. *Methods Enzymol.* **1990**, *188*, 191–202.

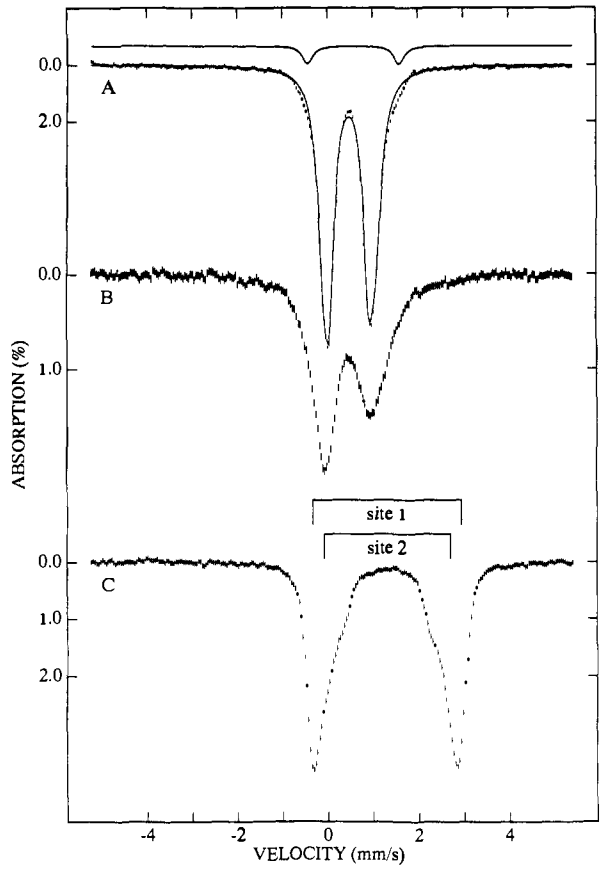

Figure 1. Mössbauer spectra of the ^{57}Fe-enriched *M. trichosporium* OB3b MMO hydroxylase: (A) oxidized hydroxylase, pH 7, in zero field at 4.2 K; (B) oxidized hydroxylase in zero field at 150 K; (C) reduced hydroxylase in zero field at 4.2 K. The solid line drawn through the data of spectrum A is a least-squares fit assuming two doublets of equal area after removing the contribution of a minority species (solid line above the data) from the raw data.

previously described.[1a,4a,17] The component B was added to samples of the mixed-valence hydroxylase (stoichiometric with active-site concentration) prior to addition of reductants.

Preparation of Reductase Samples. Three preparations of the ^{57}Fe-enriched reductase were pooled and concentrated by ion exchange and centrifugation to ~0.4 mL. The sample was partitioned between a Mössbauer cell and an EPR tube, and data for the oxidized reductase were obtained. Subsequently, the samples were recombined in a Mössbauer cell, reduced under anaerobic conditions by the addition of a 4-fold excess of sodium dithionite, and then repartitioned between the Mössbauer cell and an EPR tube.

Spectroscopic Instrumentation. X-band EPR spectra were recorded using a Varian E-109 spectrometer equipped with an E231 or E236 cavity, Oxford Instruments ESR-910 cryostat, and Hewlett Packard 436A power meter and 5350B microwave-frequency counter. Temperature, g-value calibrations, data acquisition, integration, and subtraction procedures were as previously described.[21] Spin quantitations near either $g = 2$ or $g = 4.3$ were performed under nonsaturating conditions using either $Cu(ClO_4)_2$ or Fe(III)EDTA, respectively, as standards. Mössbauer spectra were obtained on a constant acceleration instrument, and isomeric shifts are reported relative to an iron metal standard. ^{57}Fe-ENDOR spectra were recorded on a Bruker 200D EPR/ENDOR spectrometer equipped with an Oxford ESR-9 cryostat, TM_{011} cylindrical mode cavity, RF helix, Wavetek frequency synthesizer, and 300-W ENI broad-band radiofrequency amplifier with modulation at 12.5 kHz. Spectra were digitally recorded on a Bruker Aspect 2000 computer.

Results

Oxidized Hydroxylase Component. Figure 1A shows the Mössbauer spectrum of a pH 7 sample of the oxidized hydroxylase recorded at 4.2 K in zero magnetic field. The solid line drawn through the data is the sum of two quadrupole doublets[22] of equal area generated with the parameters listed in Table I. A minority species, with quadrupole splitting $\Delta E_Q = 2.0$ mm/s and isomer shift $\delta = 0.6$ mm/s accounts for ~4% of the total ^{57}Fe in the sample. As reported previously,[16a] the zero-field Mössbauer spectrum of the oxidized hydroxylase suggests the presence of an exchange-coupled Fe^{3+}·Fe^{3+} cluster with slightly inequivalent octahedral or pentacoordinate iron sites.

Spectra of the sample of Figure 1A in strong applied magnetic fields are shown in Figure 2. We have previously shown that the 6.0-T spectrum indicates a diamagnetic electronic ground state resulting from antiferromagnetic coupling of two high-spin ferric ions.[16a] High-field Mössbauer spectra recorded from 10–30 K also suggested that the exchange-coupling constant, J, was considerably smaller than previously reported for known diiron–oxo proteins. While the presence of low-lying spin multiplets was indicated, a value for J could not be extracted because intermediate relaxation rates of the electronic system gave rise to broad, unresolved spectra. In addition, fitting of the 6.0-T spectrum recorded at 4.2 K required an effective field of ~6.4 T, suggesting that the electronic ground state had some paramagnetic admixture. This deviation from strict diamagnetism becomes more pronounced at higher field. For example, the mismatched solid line drawn through the 8.0-T spectrum of Figure 2D is a calculation assuming strict diamagnetism.

The spin Hamiltonian commonly used for the description of an exchange-coupled system is

$$\mathcal{H}_{ex} = J\mathbf{S}_1\cdot\mathbf{S}_2 + \sum_{i=1}^{2}\{\beta\mathbf{S}_i\cdot\mathbf{g}_i\cdot\mathbf{H} + \mathbf{S}_i\cdot\mathbf{D}_i\cdot\mathbf{S}_i\} \quad (1)$$

where J is the isotropic exchange coupling constant and $\mathbf{S}_1$ and $\mathbf{S}_2$ are local spins; for the oxidized hydroxylase, $S_1 = S_2 = {}^5/_2$. The second and third terms describe, respectively, the electronic Zeeman interactions and the ZFS (parameters D and E; $0 \le E/D \le 0.33$) of the individual ferric ions. For a ferric site, $\mathbf{g}$ is expected to be isotropic to within 1–2%, while D-values for octahedral coordination or pentacoordination are expected to be ca. ± 1 cm^{-1}.[23] For the description of the Mössbauer spectra, eq 1 must be amended by terms describing the hyperfine interactions of the individual ^{57}Fe nuclei with the electronic environment

$$\mathcal{H}_{hf} = \sum_{i=1}^{2}\left\{\mathbf{S}_i\cdot\mathbf{a}_i\cdot\mathbf{I}_i - g_n\beta_n H\cdot\mathbf{I}_i + \frac{eQV_{zzi}}{12}[3I_{zi}^2 - I(I+1) + \eta_i(I_{xi}^2 - I_{yi}^2)]\right\} \quad (2)$$

where the $\mathbf{a}_i$ are the magnetic hyperfine tensors of the two sites; the remaining terms describe the nuclear Zeeman and electric quadrupole interactions. The Mössbauer spectra can then be computed by solving

$$\mathcal{H} = \mathcal{H}_{ex} + \mathcal{H}_{hf} \quad (3)$$

For high-spin ferric sites such as those encountered here, the magnetic hyperfine interactions are isotropic; our studies of the mixed-valence hydroxylase show the $a(Fe^{3+})$-value ≈ -30 MHz (see below). In the strong-coupling limit ($|J| \gg |D_i|$, where i

(21) (a) Aasa, R.; Vänngård, T. *J. Magn. Reson.* **1975**, *19*, 308–315. (b) Lipscomb, J. D. *Biochemistry* **1980**, *19*, 3590–3599.

(22) The spectrum cannot be fitted well to a single doublet with Lorentzian line shapes. However, the assumption of a single doublet with Voigt line shape leads to an acceptable fit. A Voigt shape would be appropriate if the ΔE_Q values were normally distributed. However, since a fit to two doublets with Lorentzian shapes represents the data well and since the hydroxylase has inequivalent sites in both the mixed-valence and fully reduced states, a model with two inequivalent sites seems most reasonable.

(23) (a) Juarez-Garcia, C.; Hendrich, M. P.; Holman, T. R.; Que, L., Jr.; Münck, E. *J. Am. Chem. Soc.* **1991**, *113*, 518–525. (b) Beck, J. L.; de Jersey, J.; Zerner, B.; Hendrich, M. P.; Debrunner, P. G. *J. Am. Chem. Soc.* **1988**, *110*, 3317–3318.

Table I. Mössbauer Parameters for the Hydroxylase Diiron Cluster

sample	T (K)	site 1 ΔE_Q[a] (mm/s)	site 1 δ (mm/s)	site 1 %	site 2 ΔE_Q[a] (mm/s)	site 2 δ (mm/s)	site 2 %
oxidized Fe^{3+}·Fe^{3+}							
pH 7	4.2	1.16	0.51	48[b]	0.87	0.50	48[b]
pH 7 + Me_2SO	4.2	1.16	0.52	50	0.91	0.51	50
mixed-valence Fe^{3+}·Fe^{2+}							
pH 7							
pH 7 + Me_2SO	150	−1.3	0.48	50	+2.4	1.19	50
reduced Fe^{2+}·Fe^{2+}							
pH 7	4.2	~3.10	~1.3	50[c]	2.4–3.0	1.3	50[c]
pH 7 + Me_2SO	4.2	~3.0	1.3	50	~2.7	1.3	50

[a] Sign not determined unless otherwise noted. [b] Remaining percentage accounted for by a minority species described in Results. [c] The 6.0-T spectrum of Figure 13 indicates ≈50% for each site.

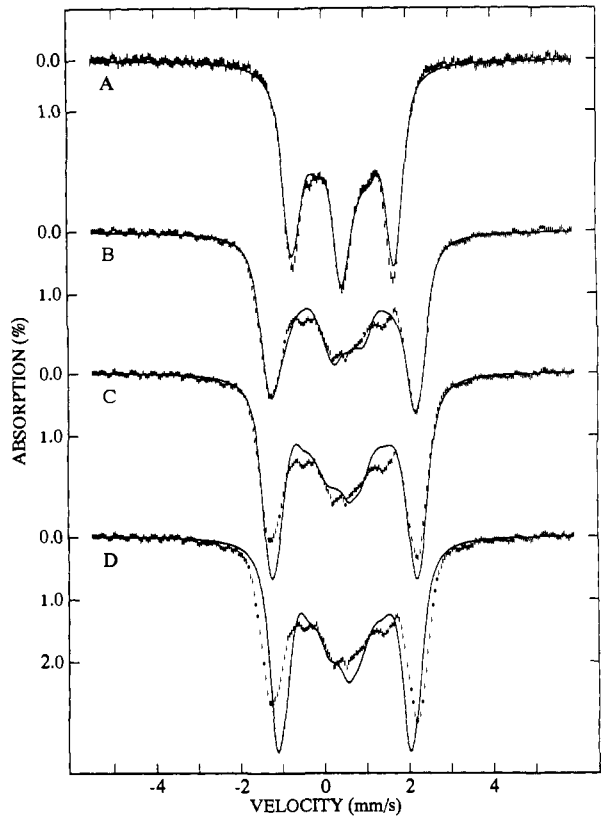

Figure 2. Mössbauer spectra of the ^{57}Fe-enriched oxidized hydroxylase recorded at 4.2 K in parallel applied fields of (A) 5.0 T and (B, C, D) 8.0 T. The solid lines in spectra A and B are spectral simulations based on eqs 1–3 using the parameter set of Table II. The solid line in spectrum C was computed by assuming diagmagnetism but by using 9.2 T for the applied field (this is equivalent to assuming an isotropic internal field of +1.2 T). The solid line in spectrum D is a spectral simulation computed assuming strict diamagnetism (zero isotropic internal field).

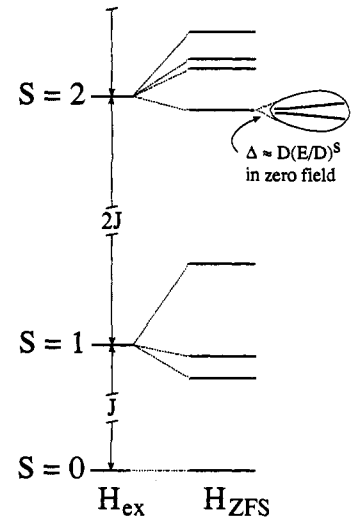

Figure 3. Energy level diagram depicting the lowest three multiplets of an antiferromagnetically coupled ($H_{ex} = JS_1 \cdot S_2$, J = 15 cm^{-1}) pair of high-spin ferric ions, $S_1 = S_2 = {}^5/_2$, and the effect of ZFS, H_{ex}, and Zeeman splitting. The EPR resonances shown in Figure 4 result from transitions within the $S = 2$ multiplet. Note that the drawing is schematic; it is not meant to imply that the EPR transitions of Figure 4 necessarily occur between the lowest levels of the $S = 2$ multiplet.

represents ZFS contributions from both ferric sites), the exchange term of eq 1 produces a series of multiplets with spins S = 0, 1, 2, 3, 4, and 5. For antiferromagnetic coupling ($J > 0$), the three lowest multiplets are diagrammed in Figure 3. The ZFS terms of eq 1 have two effects. They produce a first-order ZFS for multiplets with $S > 0$, and they mix multiplets. Scaringe and co-workers[24] have introduced a convenient scheme for analyzing the influence of the ZFS terms in the strong-coupling limit; this scheme together with the listed matrix elements provides a useful overview of a particular situation (also see ref 25). In the present work, we have diagonalized the entire spin Hamiltonian of eq 1. Using J = 15 cm^{-1}, $D_1 = D_2$ = 2 cm^{-1}, and $E_1/D_1 = -E_2/D_2$ = 0.1 (see below), we have computed the relative splittings shown in Figure 3. The relevance of this energy level scheme to the spectroscopic properties of the oxidized hydroxylase will now be described.

During the past few years, we have studied a variety of compounds with integer electronic spin that yield well-defined EPR signals.[8a,16a,b,23a,26] These studies, in particular our initial Mössbauer studies of the oxidized hydroxylase[16a] as well as recent work on the nitrogenase P-clusters,[26a] suggested that some of the low-lying multiplets of the oxidized hydroxylase may exhibit integer-spin EPR signals at X-band. The spectrum of Figure 4, obtained with the microwave magnetic field H_1 oriented parallel to the static field H, shows that this is indeed so. The oxidized hydroxylase exhibits a sharp resonance at g = 8.0, which has maximum intensity at ~30 K and which is not observed below ~10 K, indicating that it originates from an excited state. The position of the resonance strongly suggests that it originates from a doublet of an $S = 2$ manifold. Moreover, the position and sharpness of the resonance also suggest that the observed transition connects two electronic levels which have a very small energy separation in zero-field, $\Delta < 0.07$ cm^{-1}. For such resonances, the signal intensity is proportional to Δ^2.[26a,27] Since Δ is so small, it is not surprising that the signal is rather weak; in standard

(24) Scaringe, R. P.; Hodgson, D. J.; Hatfield, W. E. *Mol. Phys.* **1978**, *35*, 701–713.

(25) Bencini, D.; Gatteschi, A. In *EPR of Exchange Coupled Systems*; Springer-Verlag: New York, 1991.

(26) (a) Surerus, K. K.; Hendrich, M. P.; Christie, P. D.; Rottgardt, D.; Orme-Johnson, W. H.; Münck, E. *J. Am. Chem. Soc.* **1992**, *114*, 8579–8590. (b) Borovik, A. S.; Hendrich, M. P.; Holman, T. R.; Münck, E.; Papaefthymiou, V.; Que, L., Jr. *J. Am. Chem. Soc.* **1990**, *112*, 6031–6038. (c) Papaefthymiou, V.; Girerd, J.-J.; Moura, I.; Moura, J. J. G.; Münck, E. *J. Am. Chem. Soc.* **1987**, *109*, 4703–4710.

(27) Hendrich, M. P.; Debrunner, P. G. *Biophys. J.* **1989**, *56*, 489–506.

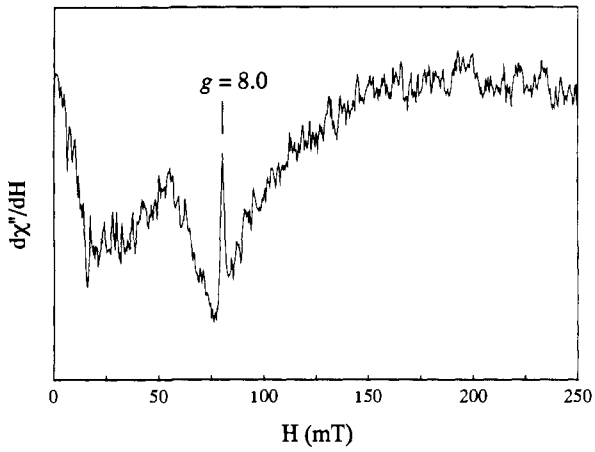

Figure 4. Parallel mode EPR spectrum of 0.7 mM oxidized hydroxylase in 50 mM MOPS, pH 7. The signal for $H < 20$ mT is from the cavity baseline. Instrumental parameters: 30 K, 2 mW at 9.079 GHz; 1-mT modulation at 100 kHz; gain 25000; dH/dt, 1.7 mT/s; filter, 0.13 s.

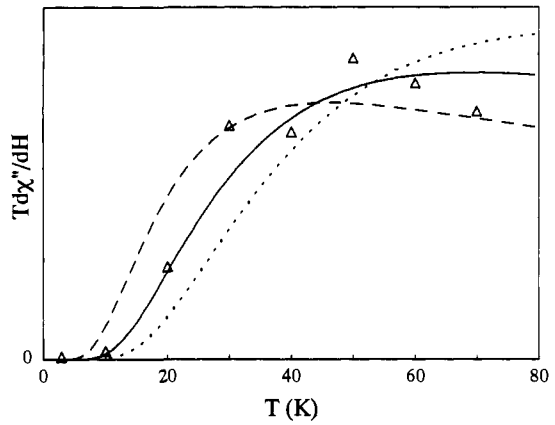

Figure 5. Temperature dependence of the $g = 8.0$ resonance of Figure 4. The lines are calculated from diagonalization of eq 1 for a signal from the $S = 2$ multiplet with $D_1 = D_2 = 0$ and $J = 10$ (- - -), 15 (—), and 20 cm^{-1} (···).

transverse mode the resonance is indistinguishable from baseline noise.

Figure 5 shows the temperature dependence (signal·T vs T) of the $g = 8.0$ signal. The computed curves, drawn for $D_i = 0$ and for $J = 10$, 15, and 20 cm^{-1}, indicate a J-value of 15 ± 5 cm^{-1}. Thus, the $S = 2$ manifold is ~ 45 cm^{-1} above the ground singlet, as shown in Figure 3. Using the temperature dependence of the signal and comparison of the intensity relative to a spin standard,[27] a value of $\Delta \approx 0.03$ cm^{-1} was obtained. This value is approximate; the full extent of the signal line shape could not be determined due to the presence of an overlapping resonance near $g = 8$.[28] However, an upper limit of $\Delta \leq 0.07$ cm^{-1} can be established from the resonance condition $(h\nu)^2 = \Delta^2 + (g_{eff}\beta H)^2$, from the observed position of the resonance ($H > 79$ mT), and from the assumption that $g_{eff} = 8$.

The identification of low-lying spin multiplets by EPR offers insight into the nature of the paramagnetic admixture into the ground state observed in the high-field Mössbauer spectra of Figure 2. Initially, we analyzed the 4.2 K spectra recorded in applied fields of 3.0, 4.0, 5.0, 6.0, 7.5, and 8.0 T with the assumption that the paramagnetic contribution to the internal magnetic field was isotropic. This can be implemented, for instance, by adjusting the applied field used for a diamagnetic simulation in order to match the overall magnetic splitting. The solid line shown for the 8.0-T spectrum of Figure 2C, computed with an adjusted applied field of 9.2 T, is an example of such an approach (this computation is equivalent to assuming the presence of an isotropic internal field of +1.2 T). Upon examination of the complete data set mentioned above, a plot of the adjusted applied field versus the actual applied field exhibited a persuasive quadratic relationship. However, while the splittings could be made to match the data quite well, we were unable to provide both a quadratic field dependence and the proper spectral intensities based on eq 1. We have therefore analyzed the spectra with the assumption that the paramagnetic contribution to the internal field was anisotropic.

Table II. Comparison of Experimental ω_i-Values with One Possible Set of Calculated ω_i-Values

	site 1			site 2		
	ω_x	ω_y	ω_z	ω_x	ω_y	ω_z
experimental	−0.06	+0.33	+0.22	+0.13	−0.35	+0.02
calculated[a]	−0.10	+0.30	−0.09	+0.10	−0.42	−0.03
ZFS only[b]	0.00	−0.03	−0.09	0.00	−0.09	−0.03

[a] The calculated values were generated using $D_1 = D_2 = +2$ cm^{-1}, $E_1/D_1 = +0.1$, $E_2/D_2 = -0.1$, $g_1 = (2.06, 2.00, 2.00)$, $g_2 = (2.00, 2.06, 2.00)$, and $J = 15$ cm^{-1}. [b] Zero-field splitting contribution to the calculated ω_i-values.

For a paramagnetic compound, the effective magnetic field acting on the ^{57}Fe nucleus is

$$H_{eff,i} = H_{int,i} + H = \frac{-\langle \mathbf{S}_i \rangle \cdot \mathbf{a}}{g_n \beta_n} + H \qquad (4)$$

where $\langle \mathbf{S}_i \rangle$ is an appropriately taken expectation value of the electronic spin. Since the excess field clearly increased with the magnetic field, we have explored a model where the expectation values of S are linear in H. Using the approximation $H_{eff,i} = (\omega_i + 1)H$ (with $i = x, y$, and z) for each of the two sites, simultaneous least-squares fitting of the entire high-field data set indeed provided a solution that reproduced both the splittings and intensities quite well. The solid lines of Figure 2A and B show the results of this fitting; the experimental ω_i-values provided by the fitting procedure are listed in Table II.

We do not yet fully understand the origin of the ω_i-values. Since J is small, we have explored whether the ω_i-values arise from mixing of the $S = 0$ ground state with excited spin multiplets by the Zeeman and ZFS terms. We have also added terms describing anisotropic $(\mathbf{S}_1 \cdot \mathbf{D}_{12} \cdot \mathbf{S}_2)$ and antisymmetric $(\mathbf{d}_{12} \cdot \mathbf{S}_1 \times \mathbf{S}_2)$ exchange to eq 1, diagonalized the electronic Hamiltonian, and calculated $\omega_{1i} = -a\langle S_{1i} \rangle / g_n \beta_n H$ and $\omega_{2i} = -a\langle S_{2i} \rangle / g_n \beta_n H$ using $a(Fe^{3+}) = -30$ MHz. These calculations reveal that the $\langle \mathbf{S}_i \rangle$ are linear in H as long as the perturbing interactions are small compared to the exchange-coupling constant J, although the mechanisms which give rise to the linear field dependence differ.[29]

In order to calculate ω_i-values approaching those obtained experimentally, mixing by the Zeeman and ZFS terms were combined with the constraint that the chosen values for D_1 and

(28) In addition to the sharp $g = 8.0$ signal and the downslope feature for $H \leq 20$ mT from the cavity baseline, there is a broad resonance near $g = 8$. This resonance has a temperature dependence similar to that of the sharp $g = 8.0$ signal, which, in addition to the position and shape, suggests that the broad resonance also results from an excited $S = 2$ manifold. Quantitation of the broad feature is only approximate due to the complication with overlapping features; nevertheless, a spin concentration roughly comparable to the protein concentration was determined. This signal originates either from a second iron cluster species (see Figure 6) or from within the same $S = 2$ manifold that produces the sharp $g = 8.0$ resonance.

(29) For the present case, the part of the Zeeman interaction that mixes the $S = 0$ and $S = 1$ states can be written as $\beta(\mathbf{S}_1 - \mathbf{S}_2) \cdot (g_1 - g_2) \cdot H/2$. Thus, mixing produces expectation values $\langle S_{1i} \rangle$ and $\langle S_{2i} \rangle$ linear in H because this perturbation is linear in H. The linear field dependence for mixing by the ZFS and antisymmetric exchange terms arises because the Zeeman term, $\beta \mathbf{S} \cdot (g + g_2) \cdot H$ splits the excited-state multiplets. This splitting produces field-dependent energy denominators in the perturbation expressions for $\langle S_{1i} \rangle$ and $\langle S_{2i} \rangle$. When these expressions are expanded in powers of H, the leading term is found to be linear in H; this term dominates for $J \approx 15$ cm^{-1} and $H \leq 8$ T.

D_2 did not conflict with the EPR data.[30] The calculated ω_i-values listed in Table II were obtained from eq 1 for $D_1 = D_2 = 2\ cm^{-1}$, $E_1/D_1 = -E_2/D_2 = 0.1$, $g_1 = (2.06, 2.00, 2.00)$, $g_2 = 2.00, 2.06, 2.00)$, and $J = 15\ cm^{-1}$. While these D-values and **g**-tensor anisotropies are somewhat larger than expected for this type of ferric site, the quoted parameters are not unreasonable.[31] For the $S = 2$ multiplet, these parameters produce a splitting $\Delta = 0.06\ cm^{-1}$, which agrees with the splitting obtained by EPR within experimental uncertainties. As shown in Table II, the contribution of the ZFS terms, listed in row 3, is rather modest. Thus, the major contribution to the ω_i-tensors has to arise from anisotropies in the Zeeman interactions. The spectra of Figure 2 show that H_{int} is predominantly positive. While the x- and y-components of the experimental ω_i-tensors are quite well reproduced by the calculation, there is a substantial mismatch for the z-components. In the framework of eq 1, it is impossible to simultaneously produce positive ω_i-values for both iron sites in all principal axis directions. The Zeeman terms produce ω_i-values such that $\omega_{1i} = -\omega_{2i}$, while ZFS and antisymmetric exchange produce ω_i-values which are on the average negative. The above treatment of the high-field data outlines a nontrivial problem rather than offering a complete solution. We do not wish to claim that our failure to provide a matching set of ω_i parameters proves that eq 1 (amended by terms describing biquadratic, anisotropic, and antisymmetric exchange) is inadequate for describing the experimental observations; however, the data of Table II suggest that some important aspect is still missing in the theory.

Figure 1B shows a zero-field spectrum of the hydroxylase recorded at 150 K. The broad features of the spectrum are indicative of paramagnetic relaxation. Sage and co-workers have reported a similar broadening for the spectra of the Fe^{3+}·Fe^{3+} cluster of purple acid phosphatase.[11a] Recent Mössbauer and integer-spin EPR studies of the P-clusters of nitrogenase may provide further insight into the phenomenon observed here. Surerus et al.[26a] have shown that one can observe paramagnetic hyperfine structure in zero-field Mössbauer spectra when two electronic levels of an integer-spin system are separated by less than $\Delta \approx 0.001\ cm^{-1}$. Under these circumstances, the two electronic states are mixed by magnetic hyperfine interactions and the nearly degenerate levels behave almost like a Kramers doublet. For multiplets with spin **S**, at least one pair of levels has $\Delta \approx D(E/D)^S$ (in the limit $E = 0$, this is the pair of sublevels with $M_S = \pm S$).[26a] Since D_1 and D_2 are typically $\pm 1\ cm^{-1}$ for the ferric sites considered here, it is highly likely that some multiplets will have a pair of levels with $\Delta < 0.001\ cm^{-1}$. These considerations, together with broadening caused by intermediate spin relaxation, may explain the features observed in the zero-field spectra of the oxidized, pH 7 hydroxylase at 150 K.

Figure 6 shows a 4.2 K Mössbauer spectrum of the oxidized hydroxylase buffered at pH 9. Comparison of the pH 7 and pH 9 samples shows the presence of a new quadrupole doublet at higher pH. This doublet is clearly discernable as shoulders at the low- and high-energy sides of the main doublet. Lack of resolution does not allow an unambiguous decomposition of the spectrum into a sum of quadrupole doublets. However, by assuming that the pH 9 spectrum contains a fraction of the pH 7 spectrum, an exploratory decomposition of the pH 9 spectrum could be made.

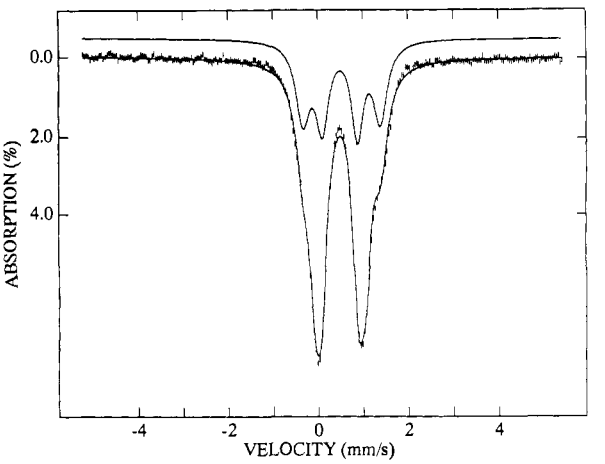

Figure 6. Mössbauer spectra of the oxidized, pH 9, ^{57}Fe-enriched hydroxylase recorded at 4.2 K in zero field. The solid line through the data represents the contribution of a pH 7 conformation of the hydroxylase with features as shown in Figure 1A (60% of the spectral intensity) and a high-pH conformation. The contribution of the two quadrupole doublets of the high-pH conformation (40% of the spectral intensity) are shown above the data.

A least-squares fit thus constrained suggested that the high-pH species consisted of two doublets, of which each contributes 20% of the total absorption (40% conversion from the pH 7 species). The doublets of the high-pH species, shown separately above the data of Figure 6, have $\Delta E_Q(3) = 1.77$ mm/s, $\delta(3) = 0.54$ mm/s, and $\Delta E_Q(4) = 0.70$ mm/s, $\delta(4) = 0.50$ mm/s, suggesting a cluster with distinct Fe^{3+} environments. Spectra obtained in applied fields up to 8.0 T had paramagnetic admixtures similar to those of the pH 7 sample. While the decomposition offered here may not be unique, it demonstrates that at least two distinct cluster forms are observed at pH 9.

Mixed-Valence Hydroxylase Component. Figure 7 shows EPR spectra of various mixed-valence forms of the hydroxylase. The spectrum of Figure 7A was obtained from a sample buffered at pH 6, while those of Figure 7B–D were recorded on pH 7 hydroxylase samples to which Me_2SO, methanol, or component B had been added before reduction. The minor species at $g = 2$, accounting for less than 0.05 spin/protein, has been previously assigned to an adventitious radical which does not correlate with enzymatic activity.[1a,c] Typically, the mixed-valence-hydroxylase EPR spectrum consists of two components with $g = (1.95, 1.86, 1.77)$ and $g = (1.98, 1.87, 1.70)$ present in an ~4:1 ratio.[17] For clarity, the contribution of the minor species has been removed by computer subtraction from the spectrum shown in Figure 7A.[32] Addition of Me_2SO or methanol causes shifts in g-values and an improvement in the spectroscopic homogeneity, as shown in Figure 7B and C, respectively. The dashed lines in Figure 7A–C are the result of spectral simulations using eq 1 for $S_1 = {}^5/_2$, $S_2 = 2$, and $J = 60\ cm^{-1}$,[4a,6] and assuming $D(Fe^{3+}) \approx 0$ and $g(Fe^{3+}) = 2.00$. The line-shape model assumes Gaussian distributions in the intrinsic g_z ($\sigma_{g_z} = 0.008$) and E/D ($\sigma_{E/D} = 0.10$) of the ferrous site. A similar line-shape model has been applied in analyses of the Fe–S clusters.[33] The characteristic parameters of the ferrous site determined from these simulations are listed in Table III. For the values of Table III, variation of the $D(Fe^{3+})$-values within $\pm 1\ cm^{-1}$ resulted in a ±10% uncertainty in the parameters of the Fe^{2+} site of the mixed-valence hydroxylase. The parameters of the ferric site cannot be uniquely determined from the spectra because the relative orientation of the molecular axes of the ferric and ferrous **D**-tensors is not known. However, proteins and model

(30) Ignoring possible (small) contributions from anisotropic exchange, the ZFS-tensor of the S = 2 multiplet is related to the intrinsic ZFS-tensors by $D = (10/21)(D_1 + D_2)$.[24] The splitting of the nearly degenerate doublet is given by $\Delta \approx 3D(E/D)^2$.

(31) By using a smaller J-value in the calculations, both the magnitude of the D_i-values and the anisotropies of the **g**-tensors could be reduced. While a smaller J would be compatible with the EPR data, Mössbauer studies indicate J cannot be smaller than 15 cm^{-1} for the following reason. In an 8.0-T field, the S = 1 state is split by the Zeeman term, lowering the energy of the $M_S = -1$ level by roughly 7.5 cm^{-1}. For $J \leq 15\ cm^{-1}$ this level would be measurably populated at 4.2 K but unpopulated at 1.5 K, giving rise to distinctly different Mössbauer spectra. However, the 8.0-T Mössbauer spectra recorded at 1.5 and 4.2 K were found to be identical.

(32) Spectra showing the contribution of this species can be found in ref 17.

(33) Bertrand, P.; Guigiarelli, B.; More, C. *New J. Chem.* **1991**, *15*, 445–454.

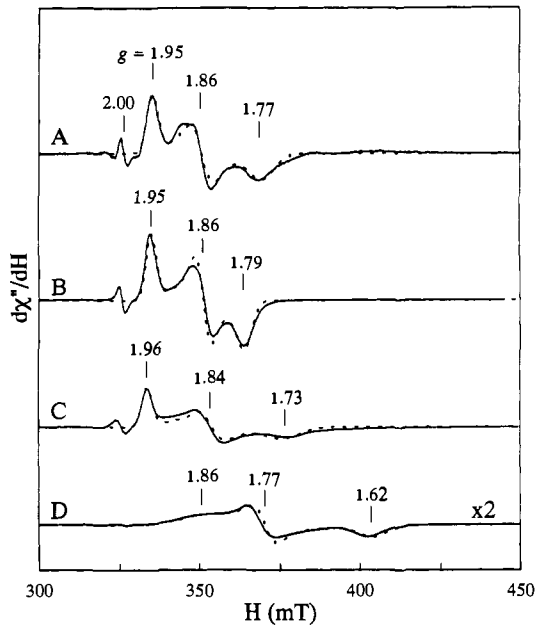

Figure 7. EPR spectra (—) and simulations (- - -) of mixed-valence hydroxylase with nothing added (A) and in the presence of 0.3 M Me_2SO (B), 50 mM methanol (C), and 2 eq of component B per diiron cluster (D). The simulation parameters are given in Table III. The line-shape model assumes Gaussian distributions of the ferrous ZFS parameters with the following widths: (A) $\sigma_{E/D} = 0.1$, $\sigma_{g_z} = 0.009$; (B) $\sigma_{g_z} = 0.008$; (C) $\sigma_{E/D} = 0.13$, $\sigma_{g_z} = 0.008$; (D) $\sigma_{g_z} = 0.019$. Protein data for B: 0.9 mM hydroxylase protein; 3.8 ± 0.3 mol of iron per mol of protein; spin quantitation of A gave 0.6 spin/protein. All spectral amplitudes are normalized to A except for D, whose amplitude has been increased by a factor of 2 for clarity. The same sample preparation of ^{57}Fe-enriched hydroxylase as B was used to generate the data of Figures 9–12. Instrumental parameters: 10 K, 20 μW at 9.134 GHz; 1-mT modulation at 100 kHz; gain, 4000; dH/dt, 0.8 mT/s.

Table III. Zero-Field Splitting Parameters and g_z of the Fe^{2+} Site of the Mixed-Valence Hydroxylase Determined from Analysis of EPR Spectra[a]

addition	D (cm^{-1})	E/D	$g_z(Fe^{2+})$
none	4.1	0.34	2.045
Me_2SO	3.8	0.25	2.044
methanol	5.2	0.31	2.037
component B	3–4		2.03–2.07

[a] All spectra were calculated by using eq 1 with $J = 60$ cm^{-1}, except for that of the component B hydroxylase complex, for which $J = 10$ cm^{-1} was used.

complexes containing mononuclear non-heme Fe^{3+} sites have $D(Fe^{3+}) \approx 0.5$ cm^{-1}.[23,34]

Addition of the component B to the mixed-valence hydroxylase gave a substantially altered EPR spectrum, as shown in Figure 7D. The simulation of the component B hydroxylase EPR spectrum does not give a unique parameter set for either the ferric or ferrous sites due to the greatly increased sensitivity of the system g-values to the ZFS of the ferric site. However, the range of acceptable values can be limited by spectral simulations as given in Table III. Figure 8 shows the dependence of the system g-values on the magnitude of the J-value; the observed g-values for the component B and uncomplexed forms of the mixed-valence hydroxylase are also indicated. For the previously determined[4a] $J \approx 10$ cm^{-1} and the set of ZFS parameters listed in the caption of Figure 8 for the component B complex of the mixed-valence hydroxylase, the simulation shown in Figure 7D was obtained. The distinctly different appearance of the component B hydroxylase EPR spectrum is a consequence of the crossing of g-values shown in Figure 8 and an overall larger intrinsic line width ($\sigma_{g_z} = 0.019$).

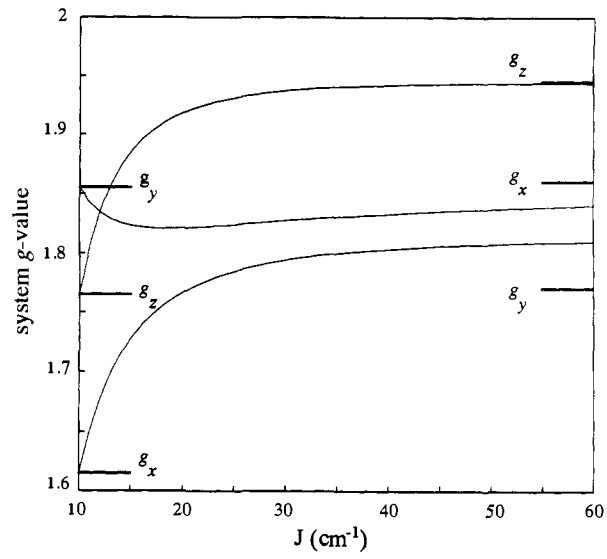

Figure 8. Effect of exchange coupling, J, on the effective g-values of the $S = {}^1/_2$ doublet for the following set of ZFS parameters: $D(Fe^{2+}) = 4.0$ cm^{-1}; $E/D(Fe^{2+}) = 0.20$; $g_x = 2.10$; $g_y = 2.14$; $g_z = 2.044$; $D(Fe^{3+}) = -0.22$ cm^{-1}; $E/D(Fe^{3+}) = 0.82$; and $g_{x,y,z}(Fe^{3+}) = 2$ under the condition that the ZFS-tensors for the two sites are collinear. The calculations are based on eq 1 in the limit of $\beta H \ll J, D_i$. The marked g-values are those observed for the mixed-valence hydroxylase with ($J = 10$ cm^{-1}) and without ($J = 60$ cm^{-1}) component B.

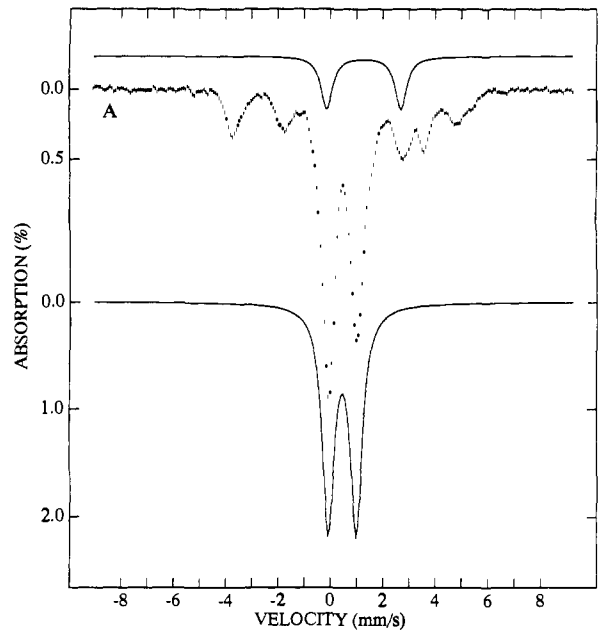

Figure 9. Redox states present in the Me_2SO-treated hydroxylase sample of Figure 7B: (A) Mössbauer spectrum recorded at 4.2 K in a parallel applied field of 20 mT. The least-squares simulations above and below the data show, respectively, the contributions of the reduced (13% of total iron) and oxidized (56% of total iron) hydroxylase. These curves were obtained by least-squares fitting of the corresponding Me_2SO-treated spectra of the oxidized and reduced hydroxylase. See the caption of Figure 7 for protein data.

The Me_2SO-treated mixed-valence hydroxylase exhibited the smallest distribution of ZFS parameters and was further studied by Mössbauer spectroscopy. Figure 9 shows a 4.2 K Mössbauer spectrum of the Me_2SO-treated mixed-valence hydroxylase recorded in a parallel field of 20 mT; this spectrum and the spectra shown in Figures 10, 11, and 12 were obtained for the same sample that yielded the EPR spectrum of Figure 7B. The potentials of the oxidized/mixed valence and mixed valence/

(34) Holman, T. R.; Juarez-Garcia, C.; Hendrich, M. P.; Que, L., Jr.; Münck, E. *J. Am. Chem. Soc.* **1990**, *112*, 7611–7618.

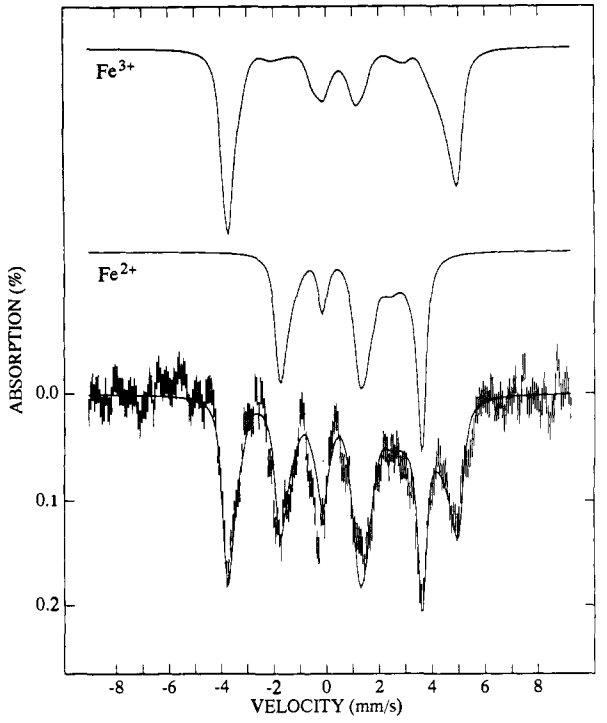

Figure 10. Mössbauer spectrum at 4.2 K of the mixed-valence hydroxylase obtained by subtracting the contributions of oxidized and fully reduced hydroxylase (solid curves in Figure 9) from the spectrum of Figure 9. The solid line drawn through the experimental data is a spin Hamiltonian simulation generated from eqs 1–3 using the parameters listed in Table IV. Simulations for the ferric and ferrous subsites are shown above the data. See the caption of Figure 7 for protein data.

reduced redox couples are such that the mixed-valence state cannot be produced in 100% yield. Figure 9 also shows the least-squares fits that represent the expected spectra of the oxidized (lower line, ~56% of total iron) and reduced (upper line, ~13% of total iron) Me_2SO-treated hydroxylase clusters. The spectrum of Figure 10 was obtained by subtracting the contributions of the oxidized and reduced clusters of the hydroxylase from the raw data of Figure 9. Due to minor uncertainties in the spectral features of the latter species, some subtraction artifacts are observed between −1.0 and +3.0 mm/s Doppler velocity. The spectra of the Me_2SO-treated mixed-valence hydroxylase exhibit paramagnetic hyperfine structure and a field dependence (parallel versus transverse field; transverse-field spectrum not shown), as expected from the EPR spectrum of Figure 7B. The appearance of paramagnetic hyperfine structure in a weak applied field implies that the electronic spin relaxation rate is slow compared to nuclear precession rates (~10–30 MHz) at 4.2 K. In contrast, the relaxation rate of the spin system of the mixed-valence hydroxylase is fast at 150 K. Consequently, the 150 K Mössbauer spectrum is composed of quadrupole doublets. Figure 11 shows a 150 K Mössbauer spectrum obtained by subtracting the appropriate contributions of the Me_2SO-treated oxidized and reduced hydroxylase. The solid line is the result of least-squares fitting of two quadrupole doublets of equal area to the data. These doublets belong to a high-spin ferric site with ΔE_Q = 1.3 mm/s and δ = 0.48 mm/s and a high-spin ferrous site with ΔE_Q = 2.4 mm/s and δ = 1.19 mm/s. This analysis of the 150 K data of Figure 11 conclusively shows that the corresponding 4.2 K spectrum of Figure 10 contains two components of equal proportions; the values of ΔE_Q and δ further indicate that these two components are intrinsically ferric and ferrous in character.

The published work on diiron–oxo proteins[8b,11a] and the analysis of the EPR data of Figure 7 show that the ground Kramers doublet of the mixed-valence forms of these proteins has some $S = {}^3/_2$ admixtures. Thus, the Mössbauer data should be analyzed by

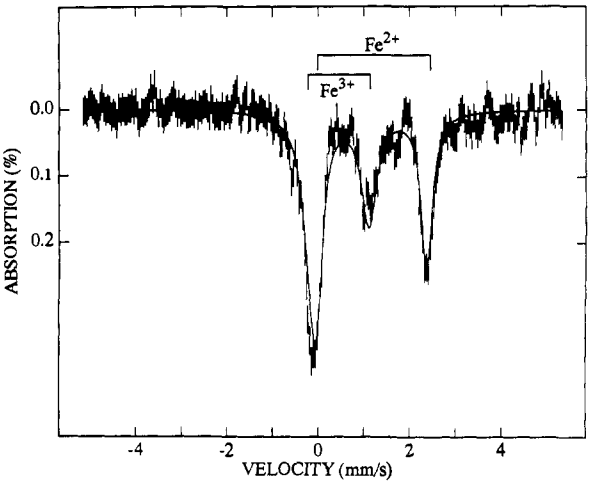

Figure 11. Mössbauer spectrum at 150 K of the mixed-valence hydroxylase obtained by subtracting the contributions of oxidized and fully reduced hydroxylase from the raw data. The solid line is a least-squares fit to two doublets of equal area. The contributions of the ferric and ferrous sites are indicated by the brackets. See the caption of Figure 7 for protein data.

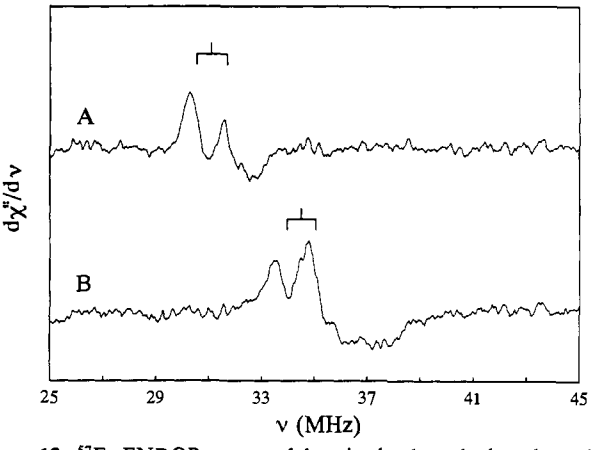

Figure 12. ^{57}Fe-ENDOR spectra of the mixed-valence hydroxylase with 0.3 M Me_2SO near (A) g_z = 1.94 and (B) g = 1.85. The signal off of EPR resonance has been subtracted. Instrumental parameters: 10 K, 50 mW at 9.423 GHz; gain 2 × 10^6; time constant, 0.2 s; 15 scans; radiofrequency sweep rate, 0.6 MHz/s; radiofrequency modulation, ±100 kHz at 12.5 kHz; radiofrequency attenuation, 10 dB; resonance field H, (A) 347 mT or (B) 365 mT. See the caption of Figure 7 for protein data.

eqs 1–3 with $S_1 = {}^5/_2$ and $S_2 = 2$. Although preliminary analysis of the Mössbauer spectra clearly indicated mixing of multiplets, we initially chose to analyze the data with the effective $S = {}^1/_2$ spin Hamiltonian

$$\mathcal{H} = \beta \mathbf{S}\cdot\mathbf{g}\cdot\mathbf{H} + \sum_{i=1}^{2}\left\{\mathbf{S}\cdot\mathbf{A}_{\mathrm{eff},i}\cdot\mathbf{I}_i - g_n\beta_n\mathbf{H}\cdot\mathbf{I}_i + \frac{eQV_{zzi}}{12}[3I_{zi}^2 - I(I+1) + \eta_i(I_{xi}^2 - I_{yi}^2)]\right\} \quad (5)$$

where the $\mathbf{A}_{\mathrm{eff},i}$ are effective A-tensors; this Hamiltonian is also more appropriate for discussing the ^{57}Fe-ENDOR spectra of Figure 12.

Figure 10 shows a spectral decomposition of the Mössbauer data into ferric and ferrous contributions. The left- and rightmost lines of the spectrum in Figure 10 belong to the ferric site. In a 6.0-T applied field these lines move to smaller absolute Doppler velocities (data not shown), implying that the magnetic hyperfine coupling constant of the ferric site is negative. In general, the A-tensors of high-spin ferric sites are expected to be

Table IV. Electronic and Hyperfine Parameters for the Mixed-Valence Hydroxylase Diiron Cluster

parameter	Fe^{3+} site	Fe^{2+} site
J (cm^{-1})	60[a]	
D (cm^{-1})	0[b]	3.8
E/D	0[b]	0.25
intrinsic g (g_x, g_y, g_z)	(2.00, 2.00, 2.00)[b]	(2.10, 2.14, 2.04)[c]
effective g (g_x, g_y, g_z)	(1.77, 1.86, 1.94)	
a[d] (MHz) (x, y, z)	(−30.5, −29.9, −28.7)	(−27.6, −23.9, −15.1)
$A_{eff,i}$[e] (MHz) (x, y, z)	(−74, −69, −63)	(+36.5, +34.3, +17.8)
$A_{eff,i}$[f] (MHz) (x, y, z)	(— 69, 62.4)	
ΔE_Q (mm/s)	−1.3	+2.5
η	1.00	0[g]
δ (mm/s)	0.53	1.24
Γ (mm/s)[h]	0.35	0.35

[a] Reference 4a. [b] By assumption. [c] $g_{x,y} = g_z - 2/\lambda(D \pm E)$ with $\lambda = -100$ cm^{-1} and $g_z = 2.04$. [d] Intrinsic a-values for the uncoupled representation of eq 2. [e] A_{eff}-values for the effective $S = {}^1/_2$ Hamiltonian of eq 5. [f] A_{eff}-values determined from ^{57}Fe-ENDOR, sign not determined. [g] Data are compatible with $0 \le \eta \le 0.6$. [h] Full width at half maximum for Lorentzian line width.

isotropic.[35] However, in order to fit the width of the outer lines of the ferric site, the $\mathbf{A}_{eff}$-tensor in the $S = {}^1/_2$ description of eq 5 required a ±10% anisotropy. This anisotropy indicates that the ZFS terms of eq 1 mix the $S = {}^3/_2$ sublevels with the ground Kramers doublet;[11a] it is therefore a measure of D_i/J, where i represents contributions from the ZFS of both ferric and ferrous sites. The spectral features of the ferrous site are strongly influenced by the large quadrupole interaction. The sharp band at +3.5 mm/s indicates that $\Delta E_Q > 0$ and that the asymmetry parameter $\eta < 0.6$; it should be stressed that η remains undetermined within the range $0 \le \eta \le 0.6$. The splitting pattern of the ferrous site also indicates that $\Delta E_Q \approx +2.5$ mm/s, i.e. ΔE_Q is nearly independent of temperature ($\Delta E_Q = 2.4$ mm/s at 140 K). With this information, the ferrous A_x and A_y are obtained from the splitting between the bands at −1.5 and +1.3 mm/s, whereas the ferrous A_z is determined from the position of the sharp band at +3.5 mm/s. Due to the presence of the oxidized and reduced hydroxylase in the sample, the resolution in the central part of the spectrum is insufficient for the direct determination of the signs of the ferrous A-tensor components from the high-field spectra.

The solid lines shown in Figure 10 were calculated by solving eqs 1–3 for $S_1 = {}^5/_2$ and $S_2 = 2$ using the parameters listed in Table IV. Virtually identical curves were obtained by solving eq 5 using the $\mathbf{A}_{eff}$ also listed in Table IV.

In the strong-coupling limit, $J \gg |D_i|$, the g- and $\mathbf{A}_{eff}$-tensors in the coupled ($S = {}^1/_2$) representation of eq 5 are related to the corresponding quantities of the uncoupled representation, eqs 1 and 2, by

$$\mathbf{g} = {}^7/_3\mathbf{g}_1 - {}^4/_3\mathbf{g}_2 \quad (6)$$

$$\mathbf{A}_1 = {}^7/_3\mathbf{a}_1 \quad (7)$$

$$\mathbf{A}_2 = -{}^4/_3\mathbf{a}_2 \quad (8)$$

For intermediate coupling, multiplet mixing by ZFS terms modifies the A-tensors of eqs 7 and 8 to produce the $\mathbf{A}_{eff}$-tensors of eq 5.[36] The mismatches between the $\mathbf{A}_i$ and $\mathbf{a}_i$ as given by eqs 7 and 8 and shown in the entries of Table IV are attributable to mixing of spin multiplets.

Figure 12 shows ^{57}Fe-ENDOR spectra of the Me_2SO-treated mixed-valence hydroxylase recorded at the low-field extremum ($g_z = 1.94$, Figure 12A) and at the middle g-value ($g = 1.85$, Figure 12B). At these field settings, sharp Zeeman doublets are observed. These resonances originate from the ferric site; those of the ferrous site are masked by proton resonances. For ^{57}Fe-ENDOR spectra, each magnetically equivalent iron atom will yield two resonances centered at $A_{eff}/2$ and split by $2g_n\beta_nH$, where $g_n = 0.18$. Thus, from the spectra of Figure 12, $A_{eff} = 62.4$ MHz at $g_z = 1.94$ and $A_{eff} = 69$ MHz at $g = 1.85$.[37] Unexpectedly, no ^{57}Fe-ENDOR resonance was observed at the high-field extremum ($g = 1.80$); similarly no ^{14}N-ENDOR resonances were observed at this field setting in our previous study.[17] The absence of a resonance at $g = 1.80$ could possibly result from a strongly anisotropic ferric A-tensor with one small component along this direction. However, the line shapes of the outer features of the Mössbauer spectrum of Figure 10 are not compatible with this hypothesis, demanding that the ferric $\mathbf{A}_{eff}$ must be isotropic to within ±12%. Alternatively, the absence of a ^{57}Fe-ENDOR resonance at $g = 1.80$ may reflect unfavorable cross-relaxation rates.

Reduced Hydroxylase Component. The previously reported zero-field Mössbauer spectra of the reduced hydroxylase consisted of two doublets, suggesting distinguishable high-spin ferrous sites.[16a] The doublet assigned to site 1, (see Figure 1C) has $\Delta E_Q \approx 3.1$ mm/s and $\delta(1) \approx 1.30$ mm/s at 4.2 K. In contrast, the spectrum of site 2 is ill-defined and cannot be represented by a single pair of Lorentzian or Voigt lines. $\Delta E_Q(2)$ is smaller than $\Delta E_Q(1)$ and temperature-dependent, and the shape of the spectrum is somewhat preparation-dependent. Spectral decompositions show that $\Delta E_Q(2)$ is distributed in a non-Gaussian manner, with ΔE_Q-values ranging from 2.4 to 3.0 mm/s. Since a fraction of the $\Delta E_Q(2)$ distribution has a quadrupole splitting similar to that of site 1, the intensity of the site 1 spectrum appears to be enhanced.

We have recorded spectra of the reduced hydroxylase over a wide range of temperatures and magnetic fields. To date, a unique parameter set that fits the high-field spectra has not been identified; at least 15 significant unknowns need to be determined even if all tensors share a common principal axis system.[38] However, even without a detailed analysis, it is clear that the reduced hydroxylase cluster contains two inequivalent Fe^{2+} sites. Figure 13 shows the Mössbauer spectrum of the reduced hydroxylase recorded at 4.2 K in a 6.0-T applied field. This spectrum consists of two components with substantially different magnetic hyperfine splittings. In order to provide an indication of the contributions of these two components, the subsite spectra

(35) Model complexes for diiron–oxo proteins show that the $\mathbf{a}(Fe^{3+})$-tensor is isotropic to within 2%.[34]

(36) Sage et al.[11a] and Bertrand[33] have given perturbation expressions which express the effective A-tensors in terms of the a_i, D_i, and J.

(37) The ENDOR resonance at $g = 1.85$ (not an EPR extremum) results from the spectral convolution of signals from molecules with many different orientations (see, for example: True, A. E.; McLean, P.; Nelson, M. J.; Orme-Johnson, W. H.; Hoffman, B. M. *J. Am. Chem. Soc.* **1990**, *112*, 651–657). Nevertheless, the sharp features suggest that the A_{eff}-value determined from Figure 12B is close to the principal axis value.

(38) Each subsite of the cluster may potentially have unique ZFS-, g-, a-, and EGF-tensors, as well as isomer shifts. These sites also interact through the exchange parameter J. Since the g-tensors are expected to be isotropic to within 10%, a detailed knowledge of the g-tensors and their orientation is not required for fitting the Mössbauer spectra. However, the spectra depend quite sensitively on most of the other parameters. As indicated in the text and in ref 16b, the iron sites of the reduced hydroxylase are ferromagnetically coupled. Thus, the parameter set described below cannot be strictly correct: if the coupling is strong, an $S = 4$ Hamiltonian has to be used; alternatively if the coupling is weak, two distinct ZFS-tensors and the J-term need to be considered. The following parameters were used to generate the simulations of Figure 13: $D = -3.4$ cm^{-1}; $E/D = 0.2$; $A_1 = (-21.4, -47.4, -12.6)$ MHz; $\Delta E_Q(1) = 3.1$ mm/s; $\delta(1) = 1.3$ mm/s; $\eta(1) = 0.2$; $\beta(1) = 30°$; $A_2 = (-5.5, -26.9, -9.1)$ MHz; $\Delta E_Q(2) = 3.1$ mm/s; $\delta(2) = 1.3$ mm/s; $\eta(2) = 0.2$; $\beta(2) = 65°$; where $\beta(1)$ and $\beta(2)$ are polar angles describing the orientations of the EFG-tensors relative to the ZFS-tensors. We wish to emphasize that the quoted parameters generate spectra which demonstrate, in our view, that the reduced hydroxylase has two distinct sites in a 1:1 ratio. We have sufficient experience with simulations of Mössbauer spectra to find a parameter set that describe a *single* spectrum and could find without much effort a different set, with distinct ZFS- and A-tensors, that also fits the 6.0-T spectrum. The determination of a unique parameter set that fits a complete data set of spectra obtained over a wide range of temperatures and applied fields requires significant further experimentation and analysis.

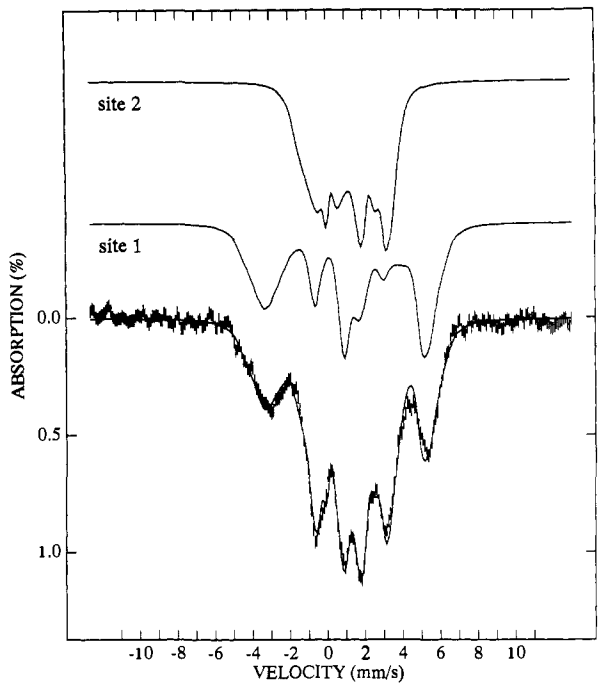

Figure 13. Mössbauer spectrum of the ^{57}Fe-enriched reduced hydroxylase recorded at 4.2 K in a 6.0-T parallel applied field. The zero-field spectrum of this sample is shown in Figure 1C. The solid lines shown above the data are subsite simulations generated from an $S = 2$ spin Hamiltonian; the solid line overlaying the data is a 1:1 sum of the subsite spectra. In a 6.0-T applied field, an $S = 2$ Hamiltonian would be appropriate for the description of the spectrum in the limit of weak ferromagnetic coupling, one of the solutions compatible with our previous integer-spin EPR study.[16b] The calculated spectra are shown to demonstrate that the reduced hydroxylase contains two distinct iron sites. The reader should not conclude that these simulations favor the weak-coupling solution.

and their sum are shown in Figure 13; a 1:1 site ratio fits the data exceedingly well. The spectra were computed with spin Hamiltonian parameters typical of high-spin ferrous sites. Spectra recorded at lower fields confirm that the species exhibiting the larger magnetic hyperfine splitting has $\Delta E_Q \approx 3.1$ mm/s, whereas the site with the smaller splitting must have a ΔE_Q centered around 2.7 mm/s. In a 6.0-T applied field, the appearance of the spectrum is dominated by the magnetic hyperfine interactions rather than the distribution in $\Delta E_Q(2)$. Our previous analysis of the integer-spin EPR transitions for the reduced hydroxylase[16b] has shown that the cluster is ferromagnetically coupled and that the two lowest spin levels of the coupled system are nearly degenerate. This near degeneracy implies that the magnetic hyperfine fields at the ^{57}Fe nuclei are uniaxial in applied fields of moderate strength, $H < 2$ T, and probably still quite anisotropic in a 6.0-T applied field. Therefore, the observation of substantially different magnetic hyperfine splittings in the Mössbauer spectra does not necessarily imply that the **a**-tensors for the two sites are drastically different. Rather, the different splittings may reflect different orientations of the two **a**-tensors relative to the anisotropic electronic system.[38]

Reductase Component. The MMO reductase contains both FAD and a [2Fe–2S] cluster which participate in the transfer of reducing equivalents from NADH to the hydroxylase.[1a,39] Proteins of similar molecular mass and cofactor content act as the oxidoreductase component for a variety of multicomponent oxygenases.[40] No detailed spectroscopic characterization of this class of iron–sulfur flavoproteins has previously been reported. Here we provide Mössbauer and EPR characterization of the [2Fe–2S] cluster of the *M. trichosporium* OB3b reductase.

(39) (a) Prince, R. C.; Patel, R. N. *FEBS Lett.* **1988**, *203*, 127–130. (b) Lund, J.; Dalton, H. *Eur. J. Biochem.* **1985**, *147*, 291–296.

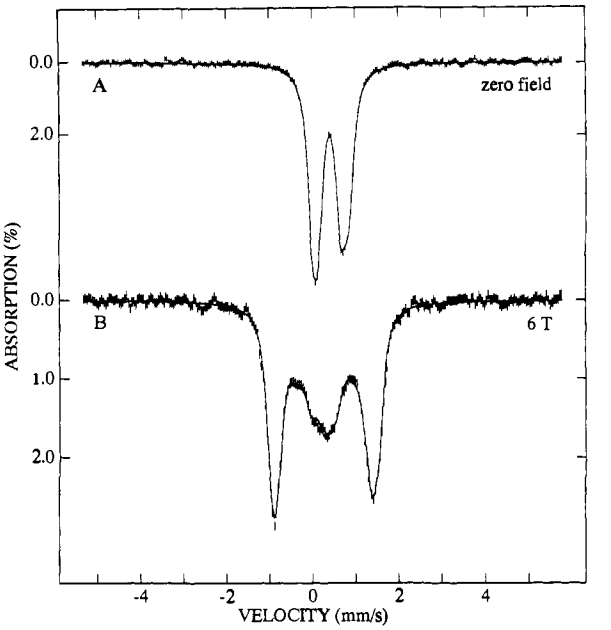

Figure 14. Mössbauer spectra at 4.2 K of the ^{57}Fe-enriched *M. trichosporium* OB3b MMO reductase recorded with (A) $H = 0$ and (B) $H = 6.0$ T. The solid lines are simulations generated using the parameters listed in Table V. Due to a lack of resolution, the sign of ΔE_Q and the value of η could not be determined reliably for the two sites; the spectra shown were computed with $\Delta E_Q(1) = 0.50$ mm/s, $\eta(1) = 0.6$, $\Delta E_Q(2) = 0.80$ mm/s, and $\eta(2) = 1$. Protein data: 2.7 mM reductase; 1 FAD and 2.1 ± 0.1 Fe/mol.

Table V. Electronic and Hyperfine Parameters for the MMO Reductase [2Fe–2S] Cluster

	site 1	site 2
oxidized $[2Fe–2S]^{2+}$		
ΔE_Q (mm/s)	0.50	0.80
δ (mm/s)	0.27	0.29
Γ^a (mm/s)	0.33	0.25
reduced $[2Fe–2S]^{1+}$		
effective g (g_x, g_y, g_z)	(1.96, 1.86, 2.05)	
$A_{eff,i}$ (MHz)	(−53.5, −48.8, −43.0)	(+13.8, +14.8, +36.5)[b]
ΔE_Q (mm/s)	0.59	−3.00
η	0	0.96[c]
δ (mm/s)	0.31	0.65
Γ^a (mm/s)	0.26	0.30

[a] Full width at half maximum for Lorentzian line width. [b] A-values for the effective $S = {}^1/_2$ Hamiltonian of eq 5. [c] Equivalent fits are obtained for a family of η- and A-values as illustrated in Figure 18.

Figure 14 shows 4.2 K Mössbauer spectra of the oxidized, ^{57}Fe-enriched reductase. The zero-field spectrum of Figure 14A consists of two doublets with parameters for ΔE_Q and δ that are typical of $[2Fe–2S]^{2+}$ ferredoxins (see Table V). The 6.0-T spectrum of Figure 14B was fitted with the assumption that the electronic ground state is diamagnetic. Note, that in contrast to the spectra of Figure 2, there is no evidence for a paramagnetic admixture; thus, the magnetic splittings are accounted for by nuclear Zeeman interactions alone. This is in accord with the results obtained from the study of other [2Fe–2S] clusters, namely, that the antiferromagnetic exchange coupling of diferric sites

(40) FAD- and [2Fe–2S]-containing electron transport proteins: (a) Batie, C. J.; Ballou, D. P.; Correll, C. C. In *Chemistry and Biochemistry Flavoenzymes*; Mueller, F., Ed.; CRC Press: Boca Raton, FL, 1992; Vol. 3, pp 543–556. (b) Powlowski, J.; Shingler, V. *J. Bacteriol.* **1990**, *172*, 6834–6840. (c) Batie, C. J.; LaHaie, E.; Ballou, D. P. *J. Biol. Chem.* **1987**, *262*, 1510–1518. (d) Correll, C. C.; Batie, C. J.; Ballou, D. P.; Ludwig, M. L. *J. Biol. Chem.* **1985**, *260*, 14633–14635. (e) Yamaguchi, M.; Fujisawa, H. *J. Biol. Chem.* **1978**, *253*, 8848–8853. (f) Bernhardt, F.-H.; Pachowsky, H.; Staudinger, H. *Eur. J. Biochem.* **1975**, *57*, 241–256. Molybdo- and [2Fe–2S]-containing enzymes characterized by EPR and Mössbauer spectroscopies: (g) Hille, R.; Hagen, W. R.; Dunham, W. R. *J. Biol. Chem.* **1985**, *260*, 10569–10575. (h) Barata, B. A.; Liang, J.; Moura, I.; LeGall, J.; Moura, J. J. G.; Huynh, B. H. *Eur. J. Biochem.* **1992**, *204*, 773–778.

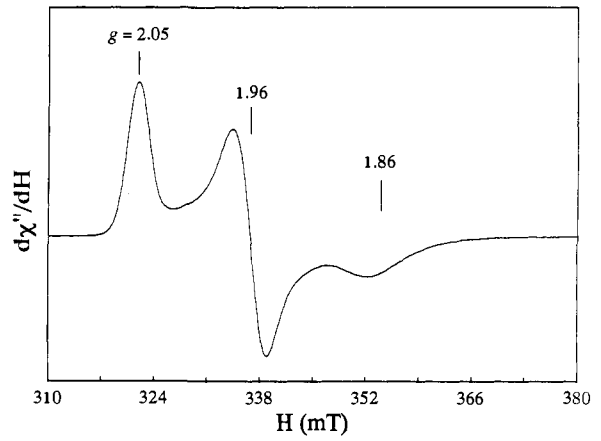

Figure 15. EPR spectrum of the sodium dithionite reduced ^{57}Fe-enriched reductase. Instrumental parameters: 7 K, 50 μW at 9.229 GHz; 1-mT modulation at 100 kHz; gain, 5000; dH/dt, 0.3 mT/s. Protein data: 2.7 mM reductase; 1 FAD and 2.1 ± 0.1 Fe/mol.

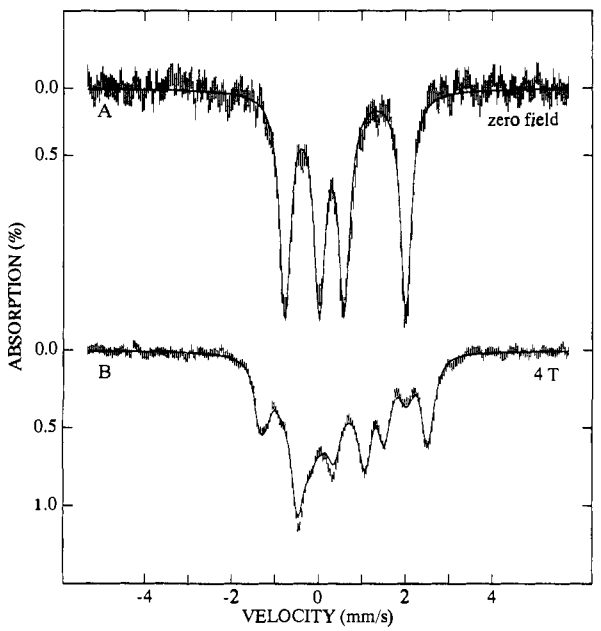

Figure 16. Mössbauer spectra at 200 K of the reduced ^{57}Fe-enriched reductase recorded in (A) 0- and (B) 4.0-T parallel applied field. The solid line in spectrum A is a least-squares fit to two quadrupole doublets using a Lorentzian line shape. The solid line in spectrum B is a spectrum calculated from eq 5 in the fast-fluctuation limit of the electronic spin using the parameters quoted in Table V.

with tetrahedral thiolate/sulfide coordination ($H_{ex} = J\mathbf{S}_1\cdot\mathbf{S}_2$, $J > 360$ cm^{-1})[41] is considerably larger than determined here for the diferric sites of the oxidized hydroxylase ($J = 15$ cm^{-1}).

Upon reduction with sodium dithionite, the EPR signal with $g_{av} = 1.96$ ($g_x = 1.86$, $g_y = 1.96$, $g_z = 2.05$) shown in Figure 15 was observed. Double integration yielded 1.06 ± 0.1 spin/mol of reductase. This EPR spectrum, obtained on the same ^{57}Fe-enriched sample used to generate the Mössbauer spectra of Figures 16 and 17, reflects the one-electron-reduced cluster $[2Fe\text{–}2S]^{1+}$. Since the analysis of such spectra has been discussed in considerable detail,[41,42] we restrict our comments here to a few salient points.

The zero-field spectrum of Figure 16A, recorded at 200 K under conditions where the electronic spin relaxes fast on the time scale of Mössbauer spectroscopy, consists of two quadrupole

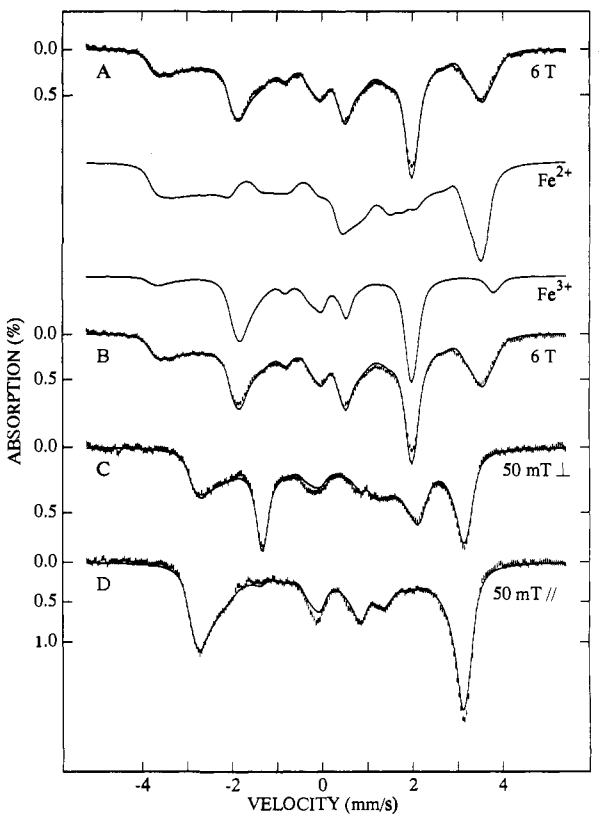

Figure 17. Mössbauer spectra at 4.2 K of the reduced ^{57}Fe-enriched reductase recorded with (A and B) 6.0-T parallel applied field; (C) 50-mT tranverse field; and (D) 50-mT parallel field. The solid line in spectrum A was calculated from eqs 1–3 using the parameters listed in Table V for $S_1 = {}^5/_2$ and $S_2 = 2$; this calculation takes mixing of multiplets into account. The solid lines in spectra B, C, and D are simulations generated from eq 5 (effective $S = {}^1/_2$ system) using the parameters listed in Table V. The calculated 6.0-T spectra for the ferric and ferrous subsites are shown above spectrum B. For clarity, the amplitude of the ferrous subsite spectrum has been increased by a factor 2.

doublets in a 1:1 ratio. The innermost doublet has parameters similar to those of site 1 of the oxidized reductase (see Table V); therefore, this site has remained high-spin ferric upon reduction. In contrast, the outermost doublet has parameters typical of those observed for high-spin ferrous iron with tetrahedral thiolate/sulfide coordination. Thus, the $[2Fe\text{–}2S]^{1+}$ cluster core contains two localized valence sites (mixed-valence class II in the Robin–Day[43] scheme).

The low-temperature Mössbauer spectra were analyzed with eq 5 assuming that all tensors in eq 5 have a common principal axis system; this assumption is justified by the high quality of the fits. The solid lines in Figures 16B and 17 are the result of spectral simulations based on eq 5 using the parameters listed in Table V. The high-field data of Figures 16B and 17 show that, in the description of eq 5, the $\mathbf{A}_{eff}$-tensor of the ferric site has negative components whereas the $\mathbf{A}_{eff}$-tensor of the ferrous site has positive components. This observation reflects the well-established antiferromagnetic coupling of $[2Fe\text{–}2S]^{+}$ ferredoxins.[41,42a] Equation 6 provides the g-tensor of the ground doublet in terms of the intrinsic g-tensors of the ferric and ferrous sites. The intrinsic g-values of the ferric ion can be assumed to be isotropic to within about 1%, with $g_{av} \approx 2.035$.[33] Using $\lambda \approx -80$ cm^{-1} for the ferrous site, the expression given in Table IV relates the ferrous g-values to the ZFS-tensor. For $g_z(Fe^{2+}) = 2.01$, $D(Fe^{2+}) = +5.1$ cm^{-1}, and $E/D = 0.25$, we obtain a calculated effective g-tensor (1.955, 1.860, 2.053) for the coupled $S = {}^1/_2$ state, in excellent agreement with the experimentally determined g-values.

(41) Sands, R. H.; Dunham, W. R. *Q. Rev. Biophys.* **1975**, *7*, 443–504.
(42) (a) Münck, E.; Debrunner, P. G.; Tsibris, J. C. M.; Gunsalus, I. C. *Biochemistry* **1972**, *11*, 855–863. (b) Fee, J. A.; Findling, K. L.; Yoshida, T.; Hille, R.; Tarr, G. E.; Hearshen, D. O.; Dunham, W. R.; Day, E. P.; Kent, T. A.; Münck, E. *J. Biol. Chem.* **1984**, *259*, 124–133.
(43) Robin, M. B.; Day, P. In *Mixed Valence Chemistry-A Survey and Classification*; Academic Press: New York, 1967; Vol. 10, pp 247–405.

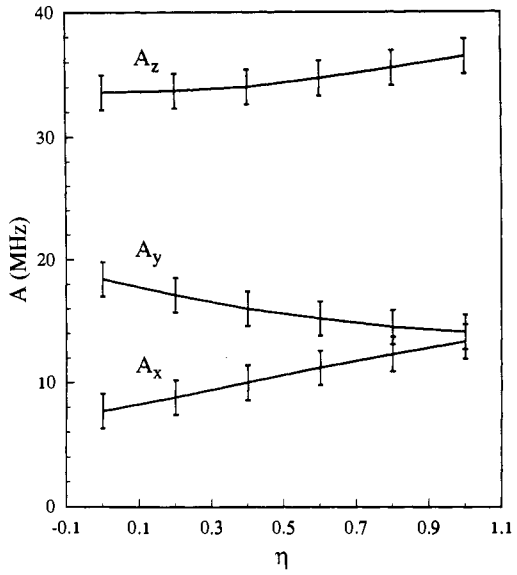

Figure 18. Correlations between the asymmetry parameter η and the A-tensor components of the ferrous site of the $[2Fe-2S]^{1+}$ cluster. A-values were obtained by fixing the value for η and then least-squares fitting the spectra of the ferrous site.

It is difficult to determine $A_{eff,x}$ and $A_{eff,y}$ of the ferrous site with precision, primarily because these parameters can be permuted with the asymmetry parameter η, which adjusts the components of the EFG-tensor along x, y, and z principal axis directions. In order to explore these correlations, the value of η was successively fixed at different values between 0 and 1 and the spectra were then least-squares fit for optimal values of $A_{eff,x}$, $A_{eff,y}$, and $A_{eff,z}$. For the range of η-values shown in Figure 18, fits of comparable quality were obtained for each triplet of the components of the ferrous A-tensor. Note that the values of $A_{eff,x}$ and $A_{eff,y}$ converge as η increases. This behavior is opposite to that predicted by the model of Bertrand and Gayda,[44] which predicts that the values of $A_{eff,x}$ and $A_{eff,y}$ will diverge as η increases.

We wish to comment briefly on one particular observation, that the magnetic hyperfine interaction of the ferric site as described by eq 5 is anisotropic. Almost identical anisotropies of the ferric site have been reported for all [2Fe–2S] proteins studied thus far. The ENDOR studies of Sands and collaborators[41] show unambiguously that these anisotropies are larger than the uncertainties of the measurements. Since the high-spin ferric ion has a ^6S ground state, one expects that the magnetic hyperfine interaction is given by the isotropic Fermi contact term. However, admixtures of higher electronic states of the ferric ion or anisotropic covalency could be responsible for the observed deviation from isotropy. Valentine[45] has noted that some of the observed anisotropy could also be attributed to mixing of multiplets by ZFS terms. Sage et al.[11a] have studied these mixing effects for the $S = {}^1/_2$ state of the diiron–oxo protein purple acid phosphatase and have shown that mixing produces **g**-tensor changes proportional to $(g_2 - g_1)D_i/J$ and **A**-tensor deviations proportional to D_i/J. Since $(g_2 - g_1)$ is typically less than 0.15, evaluation of the anisotropy of the ferric **A**-tensor provides a more sensitive probe to moderate D_i/J ratios. Although mixing of the $S = {}^1/_2$ ground state with higher multiplets is much less pronounced for the iron–sulfur ferredoxins than for diiron–oxo proteins, these effects are not completely negligible. In the absence of experimental data for the ZFS parameters of the ferric sites of $[2Fe-2S]^{1+}$ clusters, the ZFS parameters of monomeric FeS_4 sites can be used as an estimate. For ferric rubredoxin,[46a] desulforedoxin,[46b] and a synthetic FeS_4 complex,[46c] $D(Fe^{3+})$-values of +1.8, +2.2, and +2.4 cm^{-1}, respectively, have been reported. The reported J-values for $[2Fe-2S]^{1+}$ clusters range from 160 to 200 cm^{-1}.[41] By assuming $J = 160$ cm^{-1}, $D(Fe^{3+}) = 2.5$ cm^{-1}, and $E/D = 0.33$ for the reductase and by rotating the $\mathbf{D}(Fe^{3+})$-tensor 90° around the z-axis, we obtain correction factors[47] of 0.96, 0.98, and 1.08 for the x, y, and z-components of the ferric **A**-tensor. By multiplying the A-values obtained from solving eq 5 with these correction factors, we obtain A-values for the limit $D_i/J = 0$. Note that this correction reduces the anisotropy of the ferric **A**-tensor by more than a factor of 2. This example, constructed with a reasonable but fairly large D_i/J ratio, shows that mixing effects do indeed matter for $[2Fe-2S]^{1+}$ clusters. However, since the orientation of the $\mathbf{D}(Fe^{3+})$-tensor is unknown, it is not clear whether the correction reduces the anisotropy of the ferric **A**-tensor or whether the intrinsic anisotropy may actually be larger than experimentally observed. One must also conclude that mixing by ZFS terms cannot be fully responsible for the observed anisotropies of the reductase ferric **A**-tensor, unless one is willing to accept a $D(Fe^{3+}) \approx 5$ cm^{-1}.

The above discussion is based on a perturbation treatment;[11a,45] the problem can also be addressed by computing the Mössbauer spectra directly from eqs 1–3. The simulation drawn through the 6.0-T spectrum of Figure 17A was generated by diagonalization of eqs 1–3 using the parameters listed in Table V. To convert the A-values of the coupled representation shown in Table V into the a-values of the uncoupled representation, the A-values must be modified using eqs 7 and 8. The differences between the values thus obtained and the values listed in Table V arise from the mixing of system spin states by the ZFS.

Discussion

Oxidized Hydroxylase. For the diferric clusters of hemerythrin[8h] and ribonucleotide reductase[9g] ($H_{ex} = J\mathbf{S}_1\cdot\mathbf{S}_2$, $J = 270$ and 220 cm^{-1}, respectively), excited-state multiplets are sufficiently high in energy that only the ground state is appreciably populated at $T < 200$ K. However, for antiferromagnetic coupling with $J < 50$ cm^{-1}, low-lying spin multiplets are populated at temperatures where the electronic spin relaxation rate may be slow on the time scale of EPR spectroscopy. We report here for the first time, integer-spin EPR signals originating from an excited spin multiplet of a protein-bound diferric cluster. The position of the signal at $g = 8.0$ and the sharpness of the resonance shows that it originates from an $S = 2$ manifold, as indicated in Figure 3. The ZFS of the multiplet depends on the ZFS of the individual sites and is given by $D = {}^{10}/_{21}(D_1 + D_2)$ in the strong-coupling limit. The observed $g = 8$ resonance originates most likely from the pair of levels having magnetic quantum numbers $M_S = \pm 2$ in the limit $E = 0$. These levels are split by $\Delta \approx 3D(E/D)^2$, and since the magnitudes of D_1 and D_2 are on the order of ± 1 cm^{-1}, the pair of levels is accessible to X-band EPR spectroscopy. From the intensity and the line shape of the resonance, the two levels have an energy separation of $\Delta \approx 0.03$ cm^{-1} in zero field. The system g-value relative to the intrinsic g-value is given in excellent approximation as $g = 4g_z[1 - {}^3/_8(E/D)^2]$ where $g_z = (g_{1z} + g_{2z})/2$.

In the strong-coupling limit ($J \gg |D_i|$), the $S = 2$ multiplet is at energy $3J$ above the $S = 0$ ground state. By measuring the temperature dependence of the $g = 8.0$ resonance, the exchange-coupling constant J can be determined. The value obtained here,

(44) Bertrand, P.; Gayda, J.-P. *Biochem. Biophys. Acta* **1979**, *579*, 107–121.

(45) Valentine, M. *Hyperfine Interact.* **1986**, *30*, 309–335.

(46) (a) Peisach, J.; Blumberg, W. E.; Lode, E. T.; Coon, M. J. *J. Biol. Chem.* **1971**, *246*, 5877–5881. (b) Moura, I.; Huynh, B. H.; Hausinger, R. P.; Le Gall, J.; Xavier, A.; Münck, E. *J. Biol. Chem.* **1980**, *255*, 2493–2498. (c) Gebhard, M. S.; Deaton, J. C.; Koch, S. A.; Millar, M.; Solomon, E. I. *J. Am. Chem. Soc.* **1990**, *112*, 2217–2231.

(47) The correction factors were obtained in the following manner. The expectation values of the local spins, $\langle S_{1i}\rangle$ and $\langle S_{2i}\rangle$ with $i = x, y, z$, were computed using eq 1 for the lowest level; these expectation values were then multiplied by ${}^3/_7$ or $-{}^3/_4$, respectively; the results were compared with the values $\langle S_i\rangle = -{}^1/_2$ obtained from eq 5 for the strong-coupling limit.

$J \approx 15$ cm^{-1}, is substantially smaller than those reported for the clusters of hemerythrin or *E. coli* ribonucleotide reductase; this strongly suggests that the ferric sites of the oxidized hydroxylase are not linked by a μ-oxo bridge. This conclusion is in agreement with a recent EXAFS study of the *M. capsulatus* (Bath) hydroxylase,[6a] which indicated the absence of a short Fe–O bond characteristic of μ-oxo-bridged dimers. It is noteworthy that the hydroxylase cluster has a weaker exchange coupling in the oxidized state ($J \approx 15$ cm^{-1}) than the mixed-valence state ($J \approx 60$ cm^{-1}). Since Fe^{3+}·Fe^{3+} exchange interactions are generally stronger than Fe^{3+}·Fe^{2+} pairs, the couplings observed here may reflect a conformational rearrangement of the hydroxylase cluster upon reduction resulting in promotion of an antiferromagnetic exchange pathway.[46]

We have been puzzled for some time by the observation that the 4.2 K Mössbauer spectra of the oxidized hydroxylase obtained in strong applied magnetic fields could not be fit with the assumption of strict diamagnetism. Given the small J-value, one would suspect that mixing of the $S = 0$ ground state with $S = 1$ and $S = 2$ multiplets by ZFS terms or antisymmetric exchange could account for the paramagnetic admixture. However, we have found it difficult to explain that the average magnetic splitting is larger than that of a diamagnetic compound, since the ZFS and antisymmetric exchange interactions produce internal magnetic fields with predominantly negative components (see Table II for contributions by the ZFS terms). Moreover, while small anisotropies of the **g**-tensors of the ferric sites can produce components with a positive internal field at one site, they produce an equal but negative internal field for the corresponding component at the other site. Despite considerable efforts, we have not yet found a mechanism within the framework of the spin Hamiltonian approximation that explains the data in a satisfactory manner. The observation of a paramagnetic admixture in the $S = 0$ ground state is not unprecedented for an exchange-coupled Fe^{3+}·Fe^{3+} cluster, however. Spartalian and co-workers[48] have reported $J = +16.6$ cm^{-1} and a *negative* internal field of 1.1 T in a 6.0-T applied field for (μ-methoxo)[*N*,*N*′-ethylenebis(salicylamine)]iron(III)[*N*,*N*′-ethylene((*o*-hydroxylphenyl)-glycine)salicylamine]iron(III). The two ferric ions of this complex are bridged by a methoxide and a monodentate carboxylate oxygen. These authors have attributed the nonzero hyperfine field to thermal population of the $S = 1$ excited state at 4.2 K. Their explanation cannot be correct, however, for the following reason. For $J = 16.6$ cm^{-1} the components of the internal field would indeed be negative but they would be less than 0.25 T in a 6.0-T applied field; 4-fold smaller than the observed internal field. It seems plausible to us that, for a somewhat smaller J-value, these data could be explained by a combination of mixing by ZFS terms and thermal population of the $M_S = -1$ level of the $S = 1$ multiplet.

Mixed-Valence Hydroxylase. The present analysis indicates that the EPR spectral changes detected for the mixed-valence hydroxylase in the presence of Me_2SO or methanol are primarily due to a perturbation of the coordination of the ferrous site. This analysis is consistent with the conclusions previously derived from ENDOR spectroscopy.[17] Binding of the component B reduces the exchange coupling; this is apparent in the shift in observed g-values. This decrease in J may result from a perturbation of the chemical nature of the bridging species or from a conformational change promoted by the complex formation; the latter case is supported by the conformationally sensitive distribution of products observed during single turnover in the presence of the component B.[4b]

Using the parameters quoted in Table IV, we can compute the energies of excited orbital states and the components of the ^{57}Fe **a**-tensors with a simple ligand field model. By excluding ligand field symmetries lower than rhombic, the orbital ground level for octahedral or square-pyramidal ligand arrangements is of either (approximate) d_{xy} or d_{yz} symmetry (an analysis for d_{xz} is similar to that for d_{yz}). For d_{xy} or d_{yz} ground levels, second-order perturbation theory yields the following expressions for the **g**- and **A**-tensors of the ferrous site

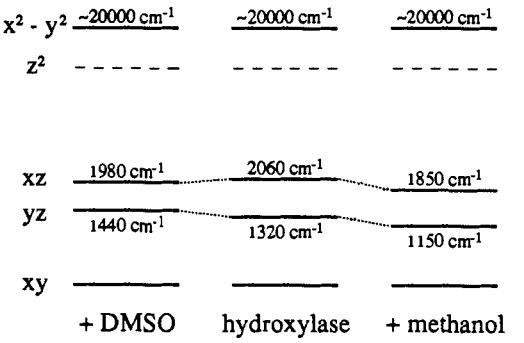

Figure 19. Ligand field energies for the ferrous ion of the mixed-valence hydroxylase cluster in the presence of perturbants. The energy levels of the d_{z^2} orbital cannot be determined from the present analysis.

$$\begin{array}{ll} d_{xy} & d_{yz} \\ g_x = g_e - 2\lambda/E_{xz} & g_x = g_e - 2\lambda\dfrac{3E_{z^2} + E_{x^2-y^2}}{3E_{z^2}E_{x^2-y^2}} \\ g_y = g_e - 2\lambda/E_{yz} & g_y = g_e - 2\lambda/E_{xy} \\ g_z = g_e - 8\lambda/E_{x^2-y^2} & g_z = g_e - 2\lambda/E_{xz} \end{array} \quad (9)$$

$$\begin{array}{ll} a_x = \alpha((g_x - 2) - {}^1/_{14} - \kappa) & a_x = \alpha((g_x - 2) + {}^1/_{7} - \kappa) \\ a_y = \alpha((g_y - 2) - {}^1/_{14} - \kappa) & a_y = \alpha((g_y - 2) - {}^1/_{14} - \kappa) \\ a_z = \alpha((g_z - 2) + {}^1/_{7} - \kappa) & a_z = \alpha((g_z - 2) - {}^1/_{14} - \kappa) \end{array} \quad (10)$$

where $\lambda \approx -100$ cm^{-1} is the spin-orbit coupling constant, E_i are the energies of the indicated orbital levels relative to the ground state, $\alpha \approx 84$ MHz,[11a,49] and $\kappa = 0.35$.[50] Provided that a second-order perturbation treatment is valid, g and D of the ferrous site are related by the perturbation expression given in Table IV. A d_{xy} orbital produces $D > 0$ whereas d_{yz} yields $D < 0$. From eq 9, the observed g-values can be reproduced by assuming a ground orbital of either d_{xy} or d_{yz} symmetry. The ambiguity can be resolved, however, by considering the magnetic hyperfine tensors. From eq 10, the calculated a-values for either a d_{xy} or a d_{yz} ground orbital are either a^{calc} = (−27.0, −23.6, −14.0) MHz or a^{calc} = (−9.0, −23.6, −32.0) MHz, respectively. Analysis of the Mössbauer spectra of Me_2SO-treated hydroxylase (Table IV) gave a^{obs} = (−27.6, −23.9, −15.1) MHz, which compares well to the a-values calculated for a d_{xy} ground orbital. The analysis of the ferrous site of the Mössbauer spectra also shows that $\Delta E_Q > 0$ and $0 \le \eta \le 0.6$. The line at +3.5 mm/s in the spectrum of Figure 10 is determined by the magnitude of the internal magnetic field (−15.1 MHz) along the largest and positive component of the electric field gradient (EFG) tensor. For both d_{xy} and d_{yz} orbitals, the EFG-tensors are axial ($\eta = 0$) and their largest, positive components are oriented along z and x, respectively. Since the corresponding internal fields ($|H_{int,i}| = |a_i|/2g_n\beta_n$) calculated for these orbitals are substantially different (a_i = −14.0 vs −9.0 MHz), the identification of a d_{xy} ground orbital level is readily made. Figure 19 shows the energies of the orbital states for the ferrous sites of the mixed-valence hydroxylase calculated from eqs 9 and 10, assuming that all spectral forms have a d_{xy} ground state similar to that of the Me_2SO-treated hydroxylase.

(48) Spartalian, K.; Bonadies, J. A.; Carrano, C. J. *Inorg. Chim. Acta* **1988**, *152*, 135–138.

(49) (a) Freeman, A. J.; Watson, R. E. In *Magnetism*; Rado, G. T., Suhl, H., Eds.; Academic Press: New York, 1965; Vol. IIA, pp 167. (b) Freeman, A. J.; Watson, R. E. *Phys. Rev.* **1964**, *133*, A1571–A1584. (c) Freeman, A. J.; Watson, R. E. *Phys. Rev.* **1962**, *127*, 2058–2076.

(50) Lang, G.; Marshall, W. *Proc. Phys. Soc., London* **1966**, *87*, 3–34.

For randomly oriented molecules as occurring in frozen solution, the Mössbauer spectra retain the spatial correlations between the **A**- and EFG-tensors. However, since the electronic **g**-tensor of the $S = {}^1/_2$ ground doublet of the Me_2SO-treated hydroxylase is fairly isotropic, spatial correlations between the **g**-tensor and the **A**- and EFG-tensors are lost. Nevertheless, by combining the spatial selectivity of ^{57}Fe-ENDOR with Mössbauer information, the ferrous **a**- and EFG-tensors can be correlated with the system **g**-tensor for the present case. Thus, using eq 5, the ENDOR resonance observed at $g_z = 1.94$, taken together with the Mössbauer results, shows that the smallest component of the ferric **A**-tensor is −62.4 MHz. With the reasonable assumption that the intrinsic **a**-tensor of the ferric site is isotropic, it follows that the $\mathbf{D}_2$-tensor chosen for the ferrous site provides the correct values for **g** and $\mathbf{A}_1$ to be used in eq 5 through mixing of multiplets. Since $|D_1|$ is certainly smaller than $|D_2|$ and since **g** is essentially independent of $\mathbf{D}_1$, it also follows that **g** and $\mathbf{A}_1$ are quite insensitive to $\mathbf{D}_1$. Therefore, $\mathbf{D}_2$ (the ferrous **D**-tensor) essentially determines the principal axis system of **g**. For a high-spin ferrous ion with a d_{xy} ground state, the z-axis of the $\mathbf{D}_2$-tensor, i.e. the axis of its largest component, is perpendicular to the plane of the orbital. Thus, for the Me_2SO-treated hydroxylase, the z-axis of the **g**-tensor of the ground $S = {}^1/_2$ state coincides with the z-axis defining the **a**- and EFG-tensors of the ferrous site.

Reduced Hydroxylase. We have not yet fully analyzed the Mössbauer data obtained for the reduced hydroxylase. In our earlier communication, we had suggested that doublet 2 (see Figure 1C of ref 16a) may be a high-spin ferrous impurity. However, the decomposition of the 6.0-T spectrum of Figure 13 into equal contributions of two subsites strongly suggests that the reduced hydroxylase cluster has two distinct ferrous sites. We can prove from the magnetization behavior that the Mössbauer spectrum of site 1 belongs to the same electronic system that gives rise to the $g = 16$ integer-spin EPR signal. Although the data are consistent with assigning the spectrum of site 2 to the same electronic system, additional experiments are required to prove this assertion. We have no evidence that the spectrum of site 2 belongs to an impurity. Rather, it would be surprising if these high-activity preparations, which contain at most 5% impurities in the oxidized state, would consistently contain an impurity in the reduced state that accounts for roughly 50% of the iron in the sample.[51] Most probably, the reduced cluster has two inequivalent ferrous sites, with one site, perhaps pentacoordinate, quite sensitive to external perturbants. This assessment is consistent with the MCD studies of the diferrous hydroxylase that show a ligand field transition at 7400 cm^{-1}.[18]

A recurring question related to MMO has been an assessment of whether the hydroxylase has one or two clusters and whether the iron sites within the clusters are structurally identical or different. Crystallographic studies of the hydroxylase from *M. trichosporium* OB3b have revealed that the unit cell has orthorhombic symmetry with one $\alpha\beta\gamma$ monomer per asymmetric unit.[52] Therefore, the hydroxylase is likely to have two-fold symmetry as well. The Mössbauer spectra of each redox state of the hydroxylase presented here are best described in terms of two spin-coupled irons in distinguishable environments. Thus, it is highly unlikely that the ligand environments of the iron atoms within a cluster are identical, as might result if a cluster were formed across a two-fold symmetry axis on a subunit boundary. Presently, the most reasonable interpretation of the Mössbauer and crystallographic data is that the dimeric hydroxylase contains two identical clusters whose individual iron sites are structurally distinct.

Conclusion

The core cluster structure of the diiron–oxo proteins allows for great potential variation in iron ligation, coordination number, coordination geometry, absolute ligand arrangement, and polarity of the cluster environment. These factors, with the addition of cluster accessibility controlled by the more global protein structure, allow ostensibly similar structures to function in disparate capacities. Here we have described the collective impact these factors have on the MMO hydroxylase cluster as manifested by characteristics such as (1) weak exchange coupling of the diferric state; (2) propensity of the spectroscopic parameters of the mixed-valence cluster to change in response to the binding of products, inhibitors, or the component B to the enzyme; (3) ferromagnetic coupling of the irons in the diferrous state; and (4) structurally differentiated irons in the two subsites of the cluster poised in each of three accessible redox states. The direct bearing of these parameters on the unique ability of MMO to activate oxygen to rapidly oxidize stable hydrocarbon bonds is only beginning to emerge. However, it is worth noting that the synthetic model complexes that mimic MMO catalysis share some of these characteristics, in particular the presence of inequivalent iron sites.[14a,b] Moreover, during the reaction leading to O–O bond breakage and oxygen activation, one of these model complexes has been shown to undergo fissure of the diiron structure.[14a] It is conceivable that equivalent chemistry might be facilitated in the hydroxylase by weakening the forces which bind the cluster irons. The small J-values observed for the diferric (and diferrous) states of the cluster may offer insight into this aspect of oxygen activation chemistry by this novel system.

Acknowledgment. This work was supported by NIH Grants GM40466 (J.D.L.) and GM22701 (E.M.), a grant from the NSF-sponsored Center for Biological Process Technology of the University of Minnesota (J.D.L.), and a contract from Amoco Corp. (J.D.L.). B.G.F. was the recipient of a USPHS Training Grant and also acknowledges a Doctoral Dissertation Fellowship from the Graduate School of the University of Minnesota. M.P.H. acknowledges an NIH Postdoctoral Fellowship (GM12996). W.A.F. was supported in part by National Institutes of Health Training Grant GM08277. We also thank Dr. P. G. Debrunner for the use of the ENDOR spectrometer with which the ^{57}Fe-ENDOR measurements were made.

(51) The essentially complete retention of enzymatic activity upon multiple cycles of sodium dithionite driven single turnover further supports the assertion that the hydroxylase cluster remains intact upon chemical reductions (see refs 1a and 5).

(52) Ohlendorf, D.; Lipscomb, J. D. Unpublished results.